WESTERN POWER DISTRIBUTION

INNOVATION

NEXT GENERATION NETWORKS

Harmonic Mitigation

Work Package Three – Algorithm design, development and implementation for multiple inverters

Report Title	:	Work Package Three – Algorithm design, development and implementation for multiple inverters
Report Status	:	Issue 1
Project Ref	:	Harmonic Mitigation
Date	:	21.06.2021

Document Control

	Name	Date
Prepared by:	Atheer Habash Grazia Todeschini (Swansea University)	02.06.2021
Reviewed by:	Zia Emin (PSC)	10.06.2021
Approved (WPD):	Jacob W.J. Lynch	21.06.2021

Revision History

Date	Issue	Status
21.06.2021	1.0	Issued

Table of Contents - Report

Glossary

Abbreviation	Term
AF	Active Filter
AG	Automatic Gain
BSP	Bulk Supply Point
CB	Circuit Breaker
FFT	Fast Fourier Transformation
LPF	Low-Pass Filter
PI	Proportional integral
PCC	Point of common coupling
PLL	Phase-locked loop
PR	Proportional resonant
PV	Photovoltaic
PWM	Pulse-width modulation
Rms	Root mean square
SCADA	Supervisory control and data acquisition
THD	Total harmonic distortion
WPD	Western Power Distribution

Executive Summary

The work reported here describes the results of Work Package 3 (referred to as WP3) of the WPD NIA Harmonic Mitigation project: the deployment of active filter (AF) functionality for multiple PV inverters. The AF functionality is added to the main role performed by the PV inverters, i.e. the delivery of power from the photovoltaic panels to the power grid. In WP2, the control algorithm operation was demonstrated for a single inverter and the harmonic reference currents were measured upstream at the point-of-common coupling, as the inverter was connected to a radial feeder effectively presenting a simple downstream fundamental and harmonic load.

In WP3, the AF functionality was deployed in multiple inverters connected to a loop. In this case, the harmonic current flows are more complex and multiple current measurement points were tested. It was concluded that the total current measured at the low voltage side of the 132/33 kV substation transformers led to the best performance, as this measurement includes the current contribution from all loads in the system.

Validating the inverters operation under various operating conditions indicated that the control system was stable in all cases, except one contingency. It was established that this behaviour was due to a resonance at the 15^{th} order harmonic, excited by a small current produced by the inverters. It was concluded that adding a filter to the input voltage measurement was necessary to give the control loops greater stability and resilience.

As already observed in WP2, when harmonic mitigation is implemented, transformer losses were exceeded under certain operating conditions. To regulate the level of harmonic injection based on transformer losses, a transformer loss coefficient (k_t) was introduced, resulting in curtailment of harmonics. As a result of the above improvements, the tests carried out in WP3 resulted in further tuning and optimisation of the control algorithm.

One of the metrics used to assess the impact of the proposed algorithm is the voltage THD at TIVE3. Across the entire observation period (October 1^{st}, 2019-October 20^{th}, 2019), the maximum reduction is approximately 45.2% from the original value. The average reduction is 34%.

During the studies and analysis of the simulation results, it was observed that when harmonic compensation was implemented, at some busbars there was an increase of current distortion, whilst observing a reduction of voltage THD. This behaviour was explained by observing that the control loops have an impact on system operation: more specifically, they cause a decrease in system impedance at the 5^{th}, 7^{th}, 11^{th}, and 13^{th} harmonic due to the presence of the PR controller.

The overall conclusion is that harmonic mitigation can be performed successfully by multiple inverters connected to the same network.

1 Introduction

This report covers the work carried out in Work Package 3 of the WPD NIA Harmonic Mitigation project.
The objectives of Work Package 3 of the harmonic mitigation project include:

- To deploy the active filter functionality on multiple inverters located on the same network.
- To optimise the effectiveness of active filter operation by coordinating the operation of the inverters.
- To develop a control functionality that allows limiting the transformer losses to be equal or below the rated value, under any operating conditions. This is achieved through a transformer loss coefficient (k_t).

The modelling environment chosen for this work is MATLAB/Simulink 2019b [1]. An overview of the system under consideration is shown in Figure 1, while more details are provided in Appendix A.

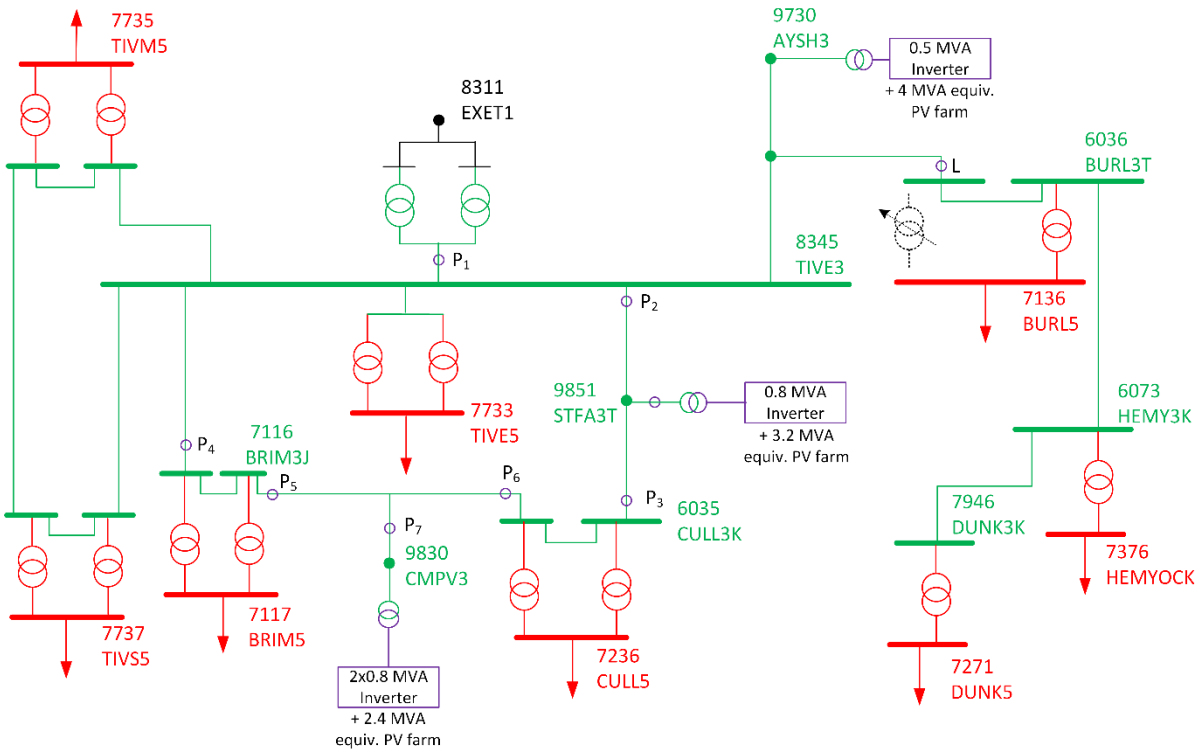

Figure 1: Overview of the Tiverton network, including the PV farms and the measurement points (P_1-P_7 and L).

This report is organised as follows:

- Section 2 provides a short description of the active filter functionality developed in Work Package 2 (WP2).
- Section 3 describes the steps undertaken to deploy and test the control algorithm on the inverters located at Stoneshill and Cullompton PV farms. Additionally, the impact on the inverter on the system impedance will be illustrated.
- Section 4 describes the tests carried out to achieve coordination of inverter operation.
- Section 5 provides an improved version of the control algorithm, including additional control loops resulting from the optimisation of the active filter operation and the tests carried out in Section 3 and Section 4.

2 Description of the control algorithm

In WP1 of this project, the basic MATLAB model of the system under consideration was developed, including the PV inverter models and their fundamental power control. In WP2, the control algorithm to perform active filter operation was developed, tested, and demonstrated for the inverter connected at Ayshford PV farm. This section provides a short description of the control strategy developed previously to make the report self-contained.

An overview of the control strategy and the harmonic mitigation algorithm are shown in Figure 2. Four quantities are fed to the controller: grid voltage (v_s), inverter dc voltage (V_{dc}), load current (i_L) and AF current (i_f). The load current is used to extract the harmonic reference currents ($i_{dq,h}$), which are used by the AF algorithm. The control algorithm consists of five main functions, as illustrated in Figure 2: dc voltage regulator, harmonic reference detection, current control, automatic gain, and Pulse Width Modulation (PWM). A standard dc voltage regulator is adopted: this regulator provides the fundamental frequency reference current (i_d^*) for the inverter, based on solar irradiance and dc reference voltage. The fundamental frequency (ω_s) is estimated from the grid voltage v_s using a phase-locked loop (PLL) and it is used to perform the dq transformation [2], [3]. The output of the current control is the reference voltages in the dq domain. After being transformed to the abc domain, the reference voltages are fed to the PWM and switching signals are obtained.

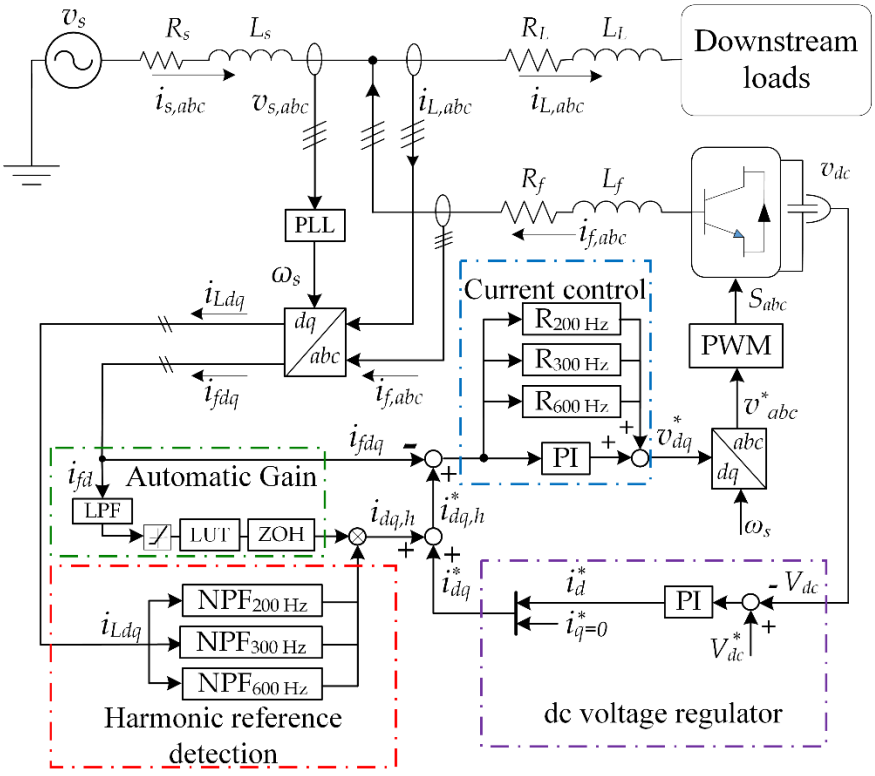

Figure 2: Overview of the control algorithm developed in Work Package 2.

The three control features specifically developed for AF operation are described more in details in the next subsections: harmonic reference detection, automatic gain and current control.

2.1 Harmonic reference detection

This function allows extracting the harmonic components $i_{dq,h}$ from the load current (i_{Ldq}). The harmonic components of interest (5th, 7th, 11th, and 13th components) are detected by using three notch peak filters (NPF): these filters pass a specified frequency component while blocking others. Both negative- and positive-sequence 5th harmonic components were considered to demonstrate the validity of the proposed approach when unbalanced harmonic components are present. For the other harmonics, only balanced operation was assumed because these harmonics are smaller, and the measurement data show negligible unbalance in the system. Therefore, the 7th and 13th harmonics were set to a positive-sequence, and the 11th harmonic was set to a negative-sequence component.

When these harmonics are transformed from abc frame to dq reference frame, three equivalent frequencies are obtained: positive sequence 5th harmonic translates in a 200 Hz component, negative-sequence 5th and positive-sequence 7th translates to 300 Hz, positive-sequence 11th, and negative-sequence 13th results in 600 Hz. Therefore, the three notch-peak filters are tuned at these frequencies.

2.2 Automatic Gain

The Automatic Gain (AG) allows modulating the amplitude of the harmonic currents injected by the inverter. This function is introduced to ensure that the rating of the PV inverter is not exceeded when harmonics are injected, and to avoid significant and frequent swings in the inverter output currents.

The AG value is calculated from the *d*-axis component of the inverter fundamental current (i_{fd}). In this project, the *q*-axis component (i_{fq}) is zero because the PV inverter operates at unity power factor, however, the proposed control will work for any power factor settings. The current i_{fd} is passed through a low-pass filter (LPF), and then a rate limiter is used to reduce the fluctuation in the current signal. The output of the rate limiter is a modified fundamental output current signal, and it is used to calculate the available capacity for harmonic compensation.

The gain value is then selected from a look-up table (LUT), and then passes through the zero-order hold (ZOH) to prevent rapid set-point fluctuations. The gain value is adjusted every 10 minutes to match the aggregation window used in weeklong 95 percentile measurements as per [4].

The calculation of the AG is illustrated through the graphs in Figure 3. The figure shows the original and modified (filtered) fundamental output current of the inverter along with the variation of the gain as a result of the current profile and the developed logic. The gain value varies between 0 and 1, where 0 means that no harmonic current can be injected, and 1 means that the full rating of the inverter is available for harmonic compensation.

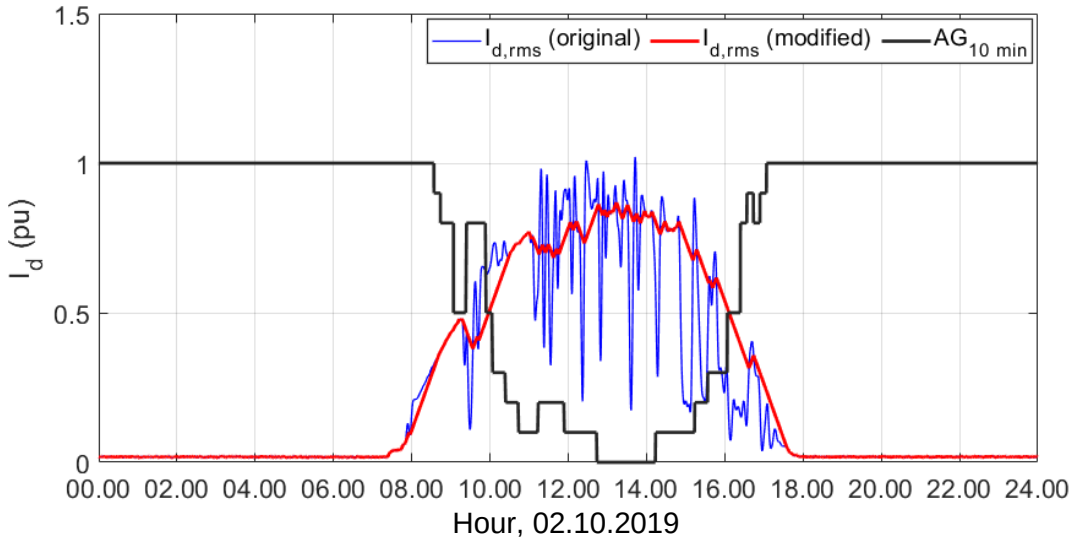

Figure 3: AG response based on variation in inverter fundamental current.

2.3 Current control

The inverter reference current ($i^*_{dq,h}$) in the dq domain includes both fundamental i^*_{dq} and harmonic components ($i_{dq,h}$). The reference current is compared with the inverter output current (i_{fdq}) and the difference is fed to the current controller. A standard PI regulator is used for the fundamental current component, but the PI regulator is unable to control the harmonic components with zero steady-state error due to bandwidth limitation [5], [6].

Therefore, for this project the standard PI-regulator is enhanced by adding three resonant controllers (R controller), as shown in Figure 2. Each one of these controllers is set for a different frequency, i.e., 200 Hz, 300 Hz, and 600 Hz. The modified PI-regulator with resonant controller (PIR) is widely employed in many applications such as active power filter, dead-time compensation, and wind power applications [5], [7], [8].

The R controller adopted in this report is described by the following transfer function in the s-domain [6], [8]:

$$G_R(s) = \frac{2K_r\omega_c s}{s^2+2\omega_c s+(h\omega_s)^2} \quad (1)$$

where K_r is the resonant gain, h refers to the selected harmonic order, ω_s is the fundamental frequency, ω_c is the cut-off frequency adopted to widen the frequency bandwidth and reduce the sensitivity of frequency variations (in this project, ω_c = 4 Hz).

2.4 Conclusions

This section provided a brief overview of the control system developed in Work Package 2 to perform active filter operation. The next sections will illustrate the steps undertaken to deploy this algorithm at various locations on the Tiverton Network.

3 Inverters operating independently as AF

The first step of the work carried out in WP3 was to deploy the control functionality described in Section 2 in all the inverters included in the model. These inverters are located at different PV farms, namely Ayshford, Stoneshill and Cullompton.

The approach taken for the deployment was to include the algorithm for AF in one inverter at the time, and then to test the algorithm under varying operating conditions to verify the stability of the controls.

In this section, each inverter is operating independently, while in Section 4 coordination and optimisation of AF operation will be studied.

3.1 Ayshford PV farm (one inverter)

The Ayshford PV farm is the only one connected to the BSP through a radial feeder, and it was considered at first because in this case the harmonic flow is unidirectional from the 11 kV loads to the upstream system, thus simplifying the algorithm development. The deployment of the AF algorithm at Ayshford PV farm was the subject of WP2 and it has been documented in the WP2 report extensively. In WP2, the harmonic reference currents used by the inverter are measured upstream of the PV farm (point L in Figure 1). In WP3 other measurements points were considered, as it will be described in Section 4.

3.2 Cullompton PV farm (one and two inverters)

As a first step, the harmonic mitigation algorithm was included in a single inverter at Cullompton PV farm. One of the main considerations was to decide the current measurement point, as Cullompton PV farm is part of a loop. Various measurement points for the load current (i_{Labc} in Figure 2) were tested, specifically P_1, P_2, P_3, P_5, and P_6 in Figure 1. Comparing the level of compensation achieved in various scenarios, it was concluded that the most effective point was P_1. After the AF functionality was deployed, various tests were run to ensure that the control was stable. These tests initially included considering static operating conditions (i.e. constant irradiance and constant loads), and then dynamic operating conditions (i.e. irradiance and load varying according to the measured data provided by WPD).

After these tests were successfully completed, the control system was deployed at the second inverter at Cullompton and the tests were repeated.

3.3 Stoneshill PV farm

The application of the control algorithm was further extended to include it in Stoneshill inverter. Firstly, the algorithm was tested with Stoneshill inverter only, and similar tests to the ones described above was conducted. Once the algorithm was verified, then AF operation for four inverters operating independently was tested.

3.4 THD calculation with four inverters operating independently

After successfully testing the individual operation of each inverter, and inverters in pairs, the simultaneous operation of all inverters (one at Ayshford, one at Stoneshill and two at Cullompton PV farm) was verified by adopting the following test conditions:

- The feedback load current measurements points are: P_1 for Stoneshill and Cullompton inverters, and L for Ayshford inverter.
- All loads and harmonics (5^{th}, 7^{th}, 11^{th}, and 13^{th}) are included.
- Background distortion from upstream 132k V network is included.
- Inverter irradiance and load variations are modelled according to the data provided by WPD.
- Automatic gain applied to all inverters.

Figure 4 shows the voltage THD at TIVE3 without and with harmonic compensation over three days in (October 1^{st}, 2019 – October 3^{rd}, 2019). More details and the percentage of reduction at the selected points and windows are given in Table 1. Additionally, Table 1 shows a comparison with the results obtained in WP2, indicating clearly the improvements achieved when four inverters are used, instead of one, to perform harmonic mitigation.

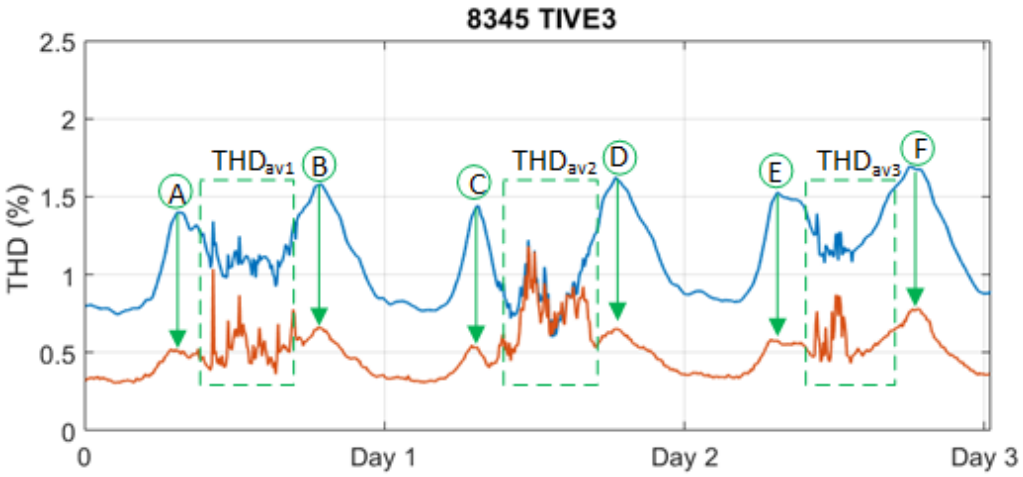

Figure 4: Voltage THD at TIVE3 before and after AF algorithm implementation.

Table 1: Voltage THD (in % of fundamental) with and without harmonic compensation deployed at four inverters. Average THD values are calculated between 9 am and 4 pm.

THD voltage profile point	THD without harmonic compensation	THD with inverters operating independently (Figure 4)	Reduction (%)	Reduction (%) with single inverter (WP2 results)
A	1.45	0.51	64.8	22.9
B	1.64	0.65	60.3	13.4
C	1.50	0.54	64.0	19.4
D	1.69	0.66	60.9	16.3
E	1.59	0.58	63.5	17.4
F	1.76	0.77	56.2	15.2
THD_{av1}	1.24	0.56	54.8	19.4
THD_{av2}	0.91	0.79	13.1	7.3
THD_{av3}	1.34	0.80	40.2	15.1

3.5 Impact of inverter on system impedance

During the analysis of the simulation results, it was observed that when harmonic compensation was implemented, at some busbars there was an increase of current distortion, while at the same time there was a reduction of voltage THD.

This behaviour is exemplified in Figure 5: the two graphs on the left show the variation of voltage and current THD at P_1: after harmonic compensation is activated at 4 am, both quantities decrease. This is an expected behaviour for a linear system. The behaviour at P_5, shown in the graphs to the right, is the opposite: the voltage THD decreases while the current THD increases. This behaviour prompted further investigation as to the reason(s) behind this observation. The investigation focused on the fact that such observation indicates a change in system impedance compared to normal operating conditions.

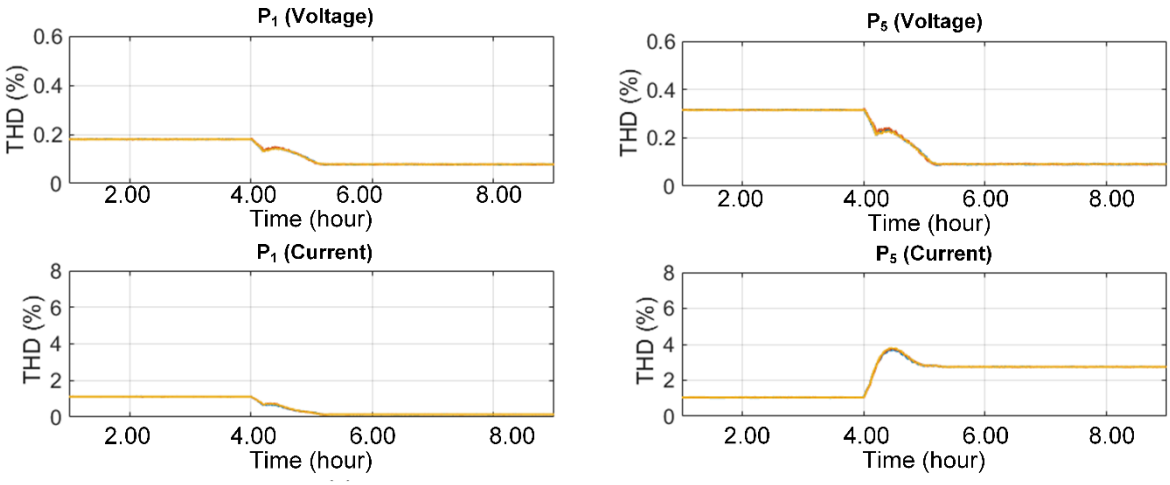

Figure 5: Voltage and current THD calculation at two locations on the Tiverton network, when the AF algorithm is activated at 4 am.

A literature review carried out indicated a possible impact of the control loop on the inverter impedance [9]. For the case of this project, the AF algorithm includes four proportional resonance (PR) controllers tuned at the 5th, 7th, 11th, and 13th harmonic, as described in Section 2. Figure 6 shows the open-loop frequency response of the inverter, indicating a high admittance at the 5th, 7th, 11th, and 13th harmonic, due to the presence of the PR controller. This response results in a reduction of the system impedance when the inverter is connected to the system and the AF algorithm is activated. This effect is exemplified in Figure 7, where the system impedance seen at Cullompton and the drop in impedance at the frequencies of interest is very clear. Frequency scans run at other locations indicates that the impact of the PR controller decreases with the increase of electrical distance from the inverter, thus matching the behaviour observed during the tests.

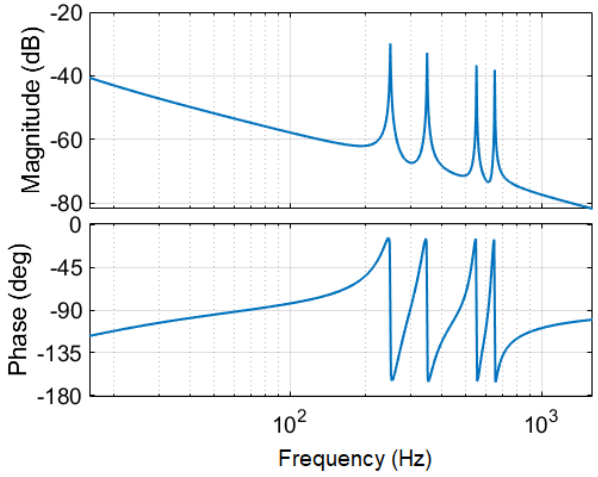

Figure 6: Inverter admittance and phase angle as function of the frequency.

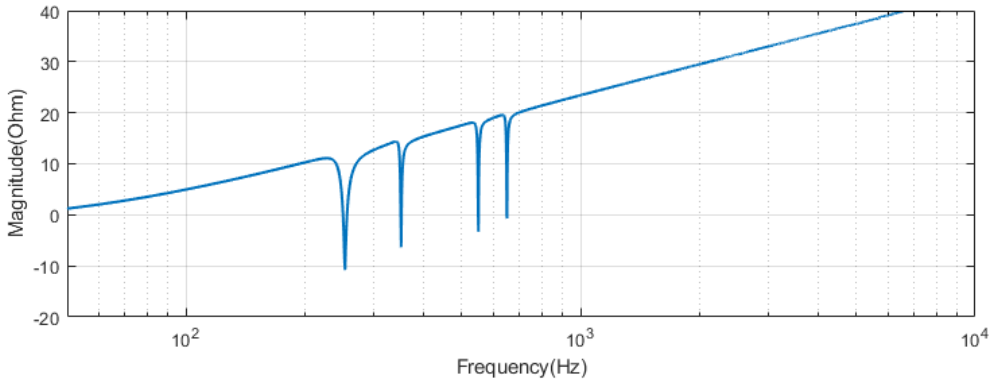

Figure 7: System impedance seen at Cullompton with AF in operation.

3.6 Conclusions

The control algorithm for harmonic mitigation developed in WP2 was deployed successfully at four inverters at the Tiverton network, and resulted in further reduction of voltage THD compared to single-inverter operation.

The impact of the inverter on system impedance was analysed and it was concluded that AF operation results in a reduction of the system impedance at the frequencies considered for harmonic compensation.

4 Coordination between inverters

Following successful deployment of the AF algorithm, the coordination and optimisation of inverter operation was analysed. The tests undertaken as part of this verification and the results are described in Sections 4.1 to 4.3, while the effect of coordination on overall THD results are provided in Section 4.4.

4.1 Current measurement point

To investigate the coordination between inverters, various current measurement points were tested as shown in Table 2. As explained in Section 2.1, this current measurement was used by the controller to calculate the reference harmonic currents.

Table 2: Load current feedback point to the inverters under each case. The locations P_1, P_2, and L are shown in Figure 1.

	Current measurement point		
	Cullompton	Stoneshill	Ayshford
Case 0	P_1	P_1	L
Case 1	P_1	P_1	P_1
Case 2	P_1	P_2	L

4.1.1 Results for various current measurement points

The inverters rms current for each case described in Table 2 is shown in Figure 8.

The first graph in Figure 8 shows Ayshford rms current: for this inverter, the current for Case 0 and Case 2 is identical because the same feedback point (L) is used. The current for Case 1 is significantly higher: this indicates that, when P_1 is used, Ayshford takes more harmonic compensation duty. This result can be explained by observing that when P_1 is adopted as a current measurement point, the total load current is included to calculate the harmonic reference. When L is used, only the loads on the radial feeder are included.

The second graph in Figure 8 shows the rms current at Stoneshill: Case 2 is associated with the P_2 measurement point and results in lower harmonic injection than using P_1 (Case 1). Similarly to the behaviour observed at Ayshford, the explanation of this results is that using P_1 results in higher harmonic reference current.

The third graph in Figure 8 shows the rms current at Cullompton: although the same feedback point is used in all cases (P_1), the inverter current is different. This result can be explained by observing that in Case 1, Ayshford is taking more harmonic compensation duties, thus lowering the harmonic content at P_1 and therefore reducing the harmonic reference current for Cullompton inverter.

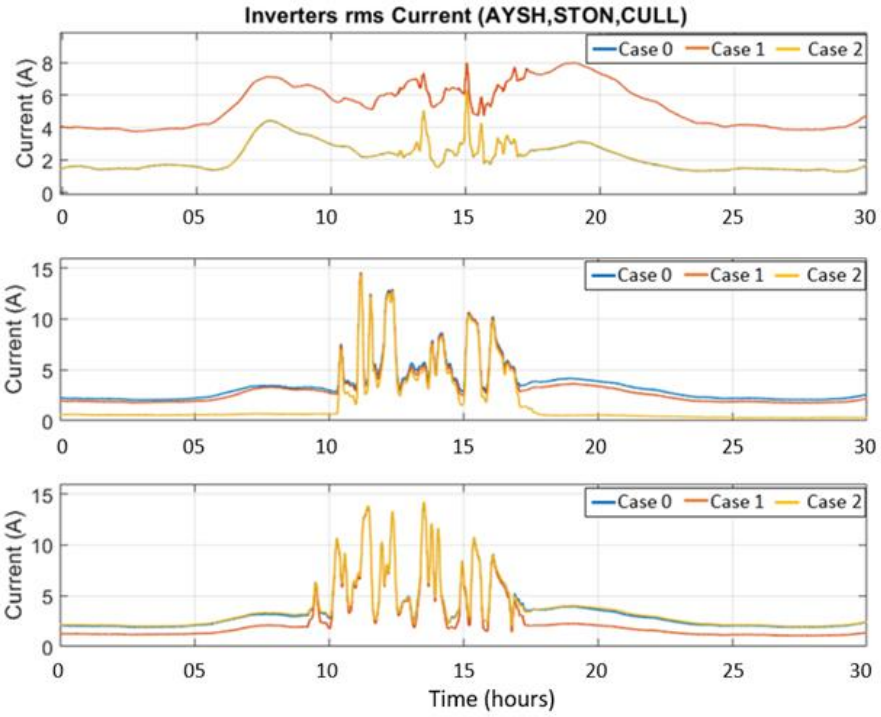

Figure 8: Inverters rms current for the cases listed in Table 2: Ayshford, Stoneshill and Cullompton inverter currents are shown.

Figure 9 shows the voltage THD measured at TIVE3 busbar under the three cases described above. The lowest THD is achieved for Case 1, when all inverters use P_1 as current measurement point (red line). The highest THD is observed under Case 2, when the compensation from Stoneshill inverter is almost zero (yellow line).

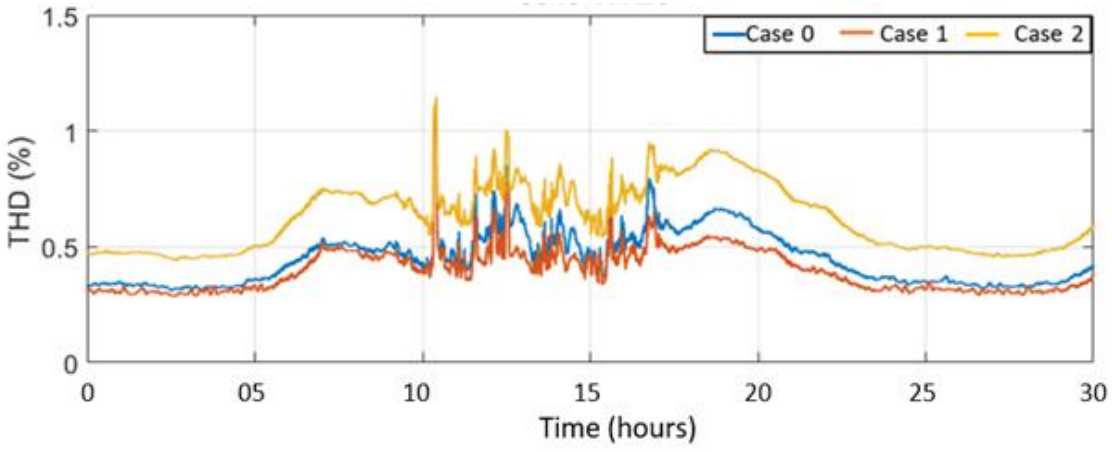

Figure 9: Voltage THD at TIVE3 for the cases listed in Table 2.

These tests prove that it is possible to use different measurements points for the inverters, and as a result the individual contribution to harmonic compensation will vary. Switching between different feedback points while the inverters are connected to the system is also possible. However, it is not recommended due to the introduction of transient components at the instants of switching.

4.2 Robustness validation

After choosing the current measurement location, robustness validation was carried out. This included testing the harmonic mitigation algorithm under various operating scenarios:

S1. Disabling harmonic injection at TIVE5.
S2. Doubling harmonic injection at DUNK5.
S3. Modifying the phase shift of harmonic injection at TIVS5.
S4. Disabling compensation from Stoneshill inverter.
S5. Setting Ayshford inverter fundamental current to zero.
S6. Disconnecting BRIM5 load and harmonic injection.
S7. Switching off the second inverter at Cullompton.
S8. Doubling the upstream voltage distortion.

Figure 10 shows the locations of the eight operating scenarios on the Tiverton network single-line diagram.

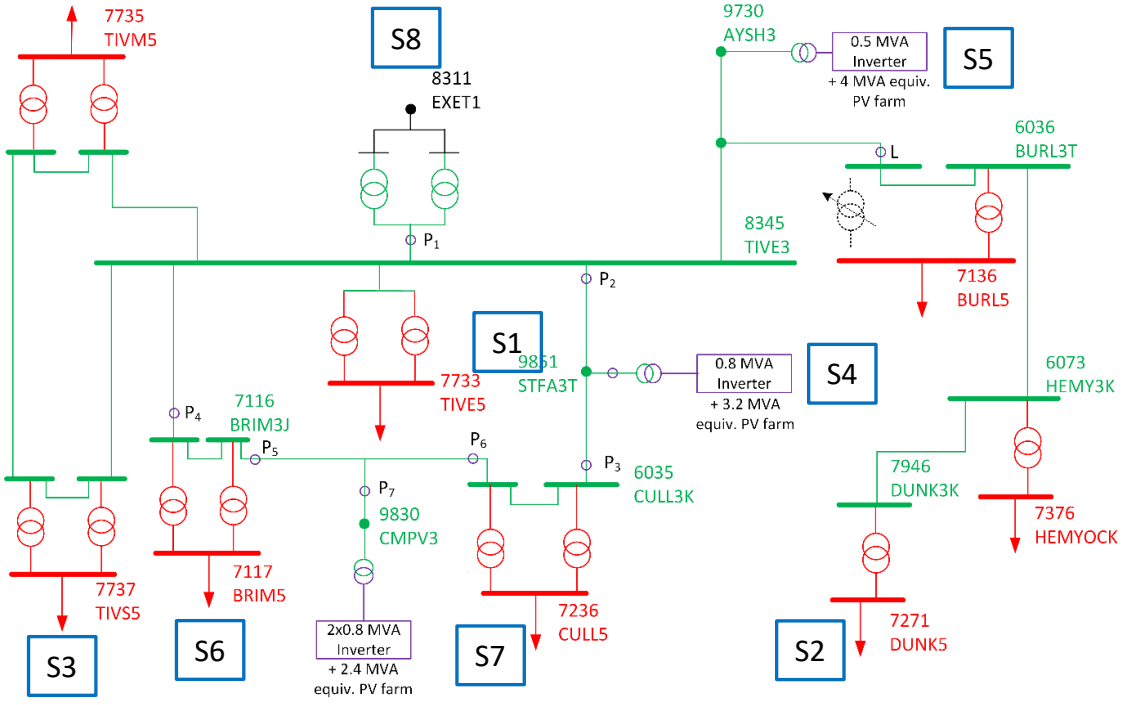

Figure 10: Location of the operating scenarios used for robustness validation.

4.2.1 Results for robustness validation

The inverter rms current and voltage THD at TIVE3 are shown in Figure 11 and Figure 12, respectively. The total simulation time for this test was 55 h, and each scenario was applied at different times, as indicated in brackets.

S1. Disabling harmonic injection at TIVE5 (t=2.5 – 5 h)

When the load harmonics at TIVE5 is disabled, the total harmonic distortion seen at TIVE3 is reduced, hence the harmonic injection by Cullompton and Stoneshill inverters with compensation is reduced. For this test, Ayshford inverter current is not affected because it is using point L as load current measurement point.

S2. Doubling harmonic injection at DUNK5 (t=7.5 – 9 h).

The injection from Ayshford inverter increases due to the higher harmonic currents measured at point L. The harmonic injection from Cullompton and Stoneshill inverter is not affected by this change.

S3. Modifying the phase shift of harmonic injection at TIVS5 (t=17.5 – 20 h).

When the harmonic source at TIVS5 is out-of-phase compared to the other harmonic sources, the total harmonics seen at TIVE3 is reduced, due to harmonic cancellation. As a result, the harmonic injected by Stoneshill and Cullompton inverters is reduced. Ayshford inverter current is not affected under this scenario.

S4. Disabling compensation from Stoneshill inverter (t=25 – 27.5 h).

The contribution in harmonic compensation from Cullompton inverter increases when Stoneshill inverter is disabled, but it cannot take all harmonic duties, therefore, the voltage THD at TIVE3 increases. Ayshford inverter is not affected because it is using point L as a current measurement point.

S5. Setting Ayshford inverter fundamental current to zero (t=35 – 37.5 h).

The automatic gain detects the drop in fundamental current and harmonic compensation increases since the inverter has free capacity. The other inverters are providing fundamental power and there is no room for harmonic compensation. The voltage THD is reduced because there is additional compensation from the Ayshford inverter.

S6. Disconnecting BRIM5 load and harmonic injection (t=40 – 42.5 h).

The load and harmonic source at BRIM5 are disconnected. As a result, the voltage THD at TIVE3 drops. The harmonic injection from Stoneshill and Cullompton inverters drop as well. Two spikes are noticeable in voltage THD at the beginning and end of load disconnection, which are caused by the dynamic behaviour of the load model and the block used to calculate voltage THD in simulation.

S7. Switching off the second inverter at Cullompton (t=45 – 47.5 h).

As one inverter is switched off, the voltage THD increases. The contribution in harmonic compensation from the other inverters increases.

S8. Doubling the upstream network distortion (t=47.5 – 50 h).

This scenario is applied at the background distortion by doubling the voltage harmonic injection. The voltage THD at TIVE3 is increased, while there is no change in the inverter current injection. The reason behind this behaviour was investigated and it was found out that doubling the background distortion results in a minimal increase of the harmonic currents at P_1, thus not affecting significantly the harmonic reference current calculation.

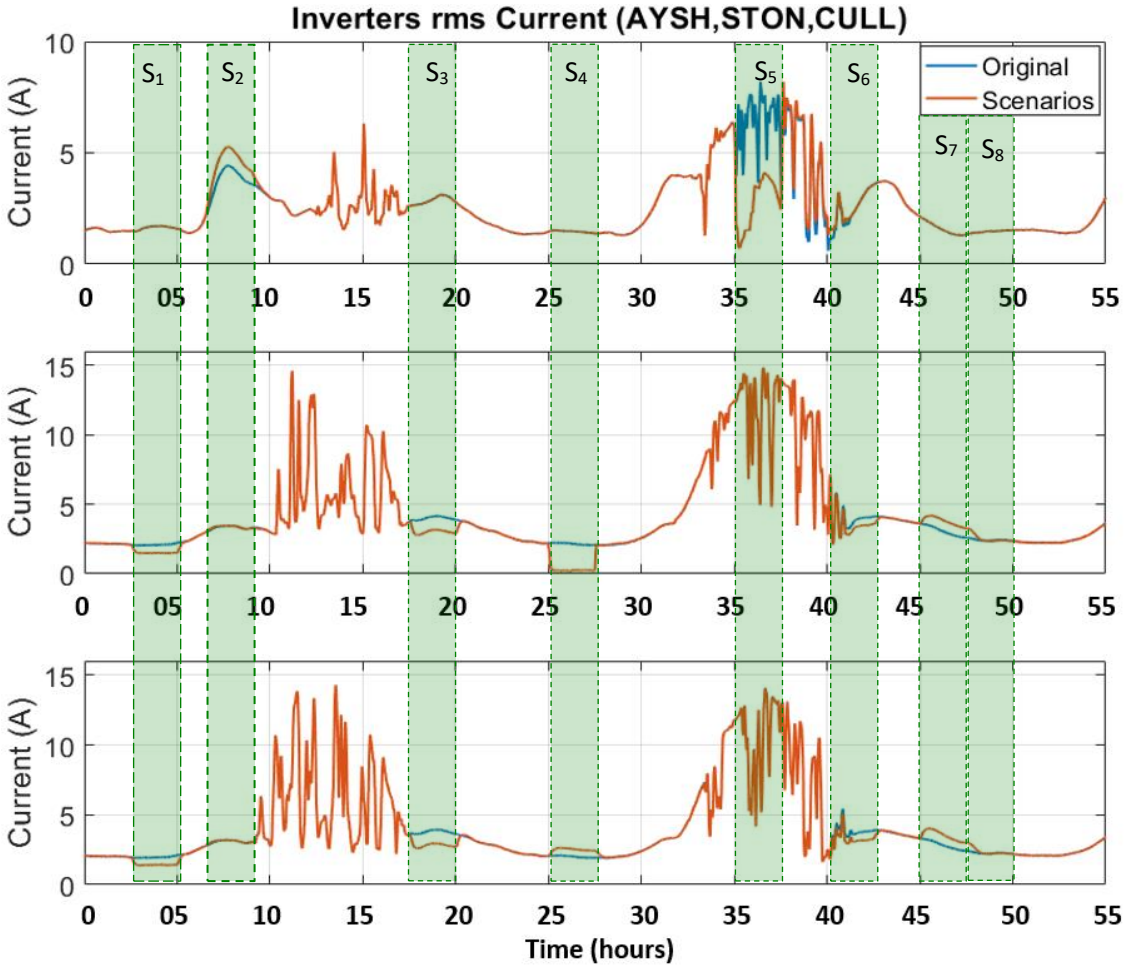

Figure 11: Inverters rms current when robustness scenarios are applied.

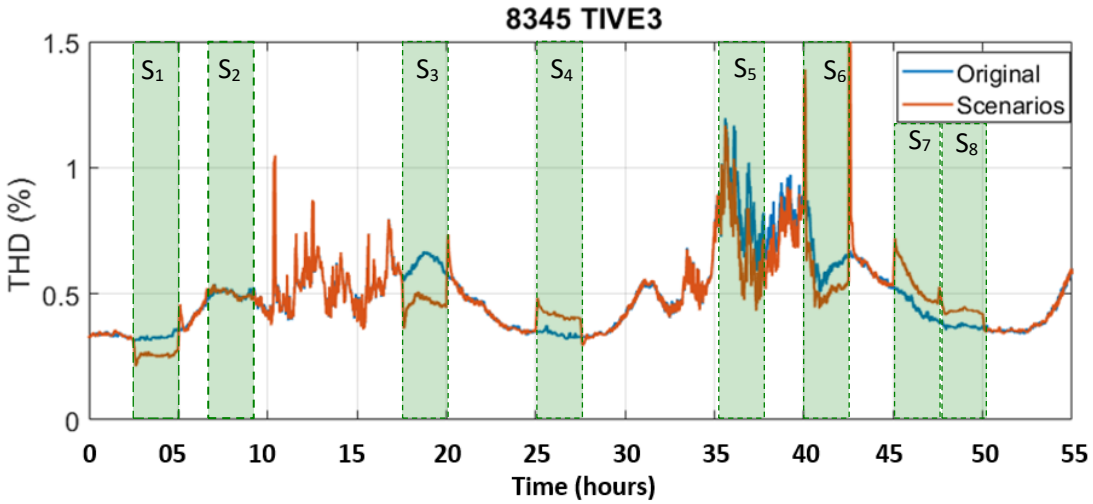

Figure 12: Inverters rms current under robustness scenarios.

4.3 Contingency cases

Three contingency tests were considered, where the loop including Cullompton PV farm and Stoneshill PV farm was open at different points:

- P_2 open between 6.00 and 10.00,
- P_3 open between 12.00 s and 16.00,
- P_4 open between 18.00 and 22.00.

P_2 and P_4 correspond to the location of circuit breaker 2L5 and 3L5, respectively. The first and third test above were the same studied in WP1, while the second case was added because P3 is located between Stoneshill and Cullompton, and therefore disconnecting this point results in testing the two inverters operating as if they were connected on two separate feeders.

4.3.1 Results for contingency cases

The voltage THD profile at the BSP for the original case (blue) and for the contingency cases (orange) is shown in Figure 13. One can observe that the voltage THD between 6 am and 10 am increases when compared to the original case. This time period corresponds to the first contingency. For the other contingencies, the THD was the same, except for small spikes at 12.00 and 16.00 due to the switching transients. The increase of voltage THD during the first contingency was caused by a 15^{th} harmonic resonance that resulted in amplification of the 15^{th} harmonic voltage component at the BSP.

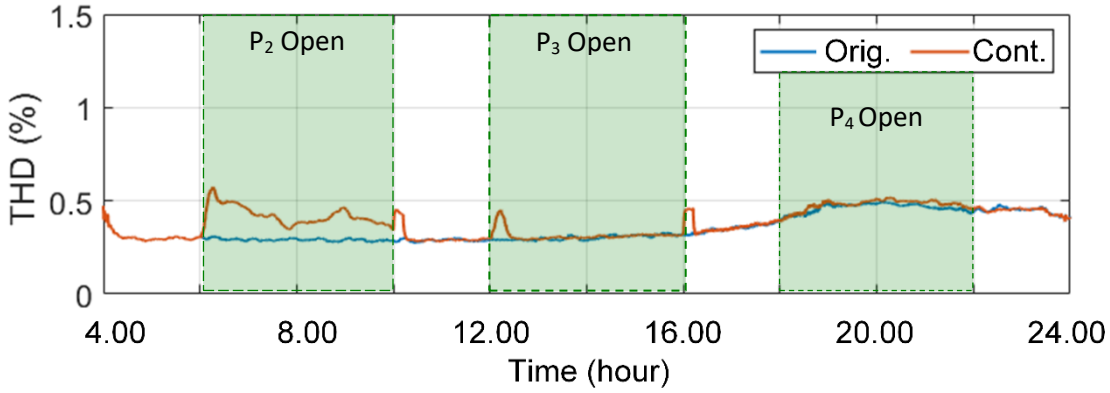

Figure 13: Voltage THD at TIVE3: original case (blue line) and contingency (orange line), with the original algorithm.

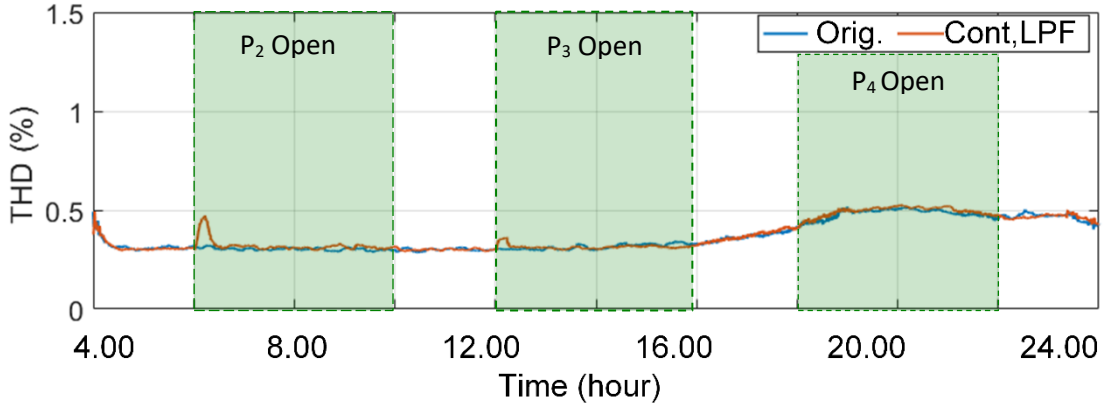

Figure 14: Voltage THD at TIVE3: original case (blue line) and contingency (orange line), with the modified algorithm (details provided in Section 5.1).

The above behaviour was mitigated by adding a low-pass filter (LPF) to the voltage THD measurement. This implementation is explained more in details in Section 5.1. Figure 14 shows a comparison of the original (without contingency) voltage THD and with the three contingency cases when the LPF is applied. One can observe that the effect of contingency cases on voltage THD is small, apart from a short transient following switching of the circuit breaker.

The currents measured at P_2, P_3 and P_4 during contingency are shown in Figure 15. During the first contingency, when P_2 was open, Stoneshill current (including fundamental and harmonic components) flowed via P_3. The current supplied to the loads through P_4, and therefore P_4 current increased as shown in Figure 15.

During the second contingency, the feeder was open at P_3 (downstream Stoneshill PV farm): in this case, Stoneshill current flowed through P_2 and the currents supplied to the loads through P_4.

For the last contingency, when P_4 is open, the loads were supplied through P_2 and P_3, hence the current increased in these points as shown Figure 15.

The THD calculation and currents waveforms indicate that the control system is stable under all operating conditions, and changes in current flow take place almost instantaneously and with no overshoot.

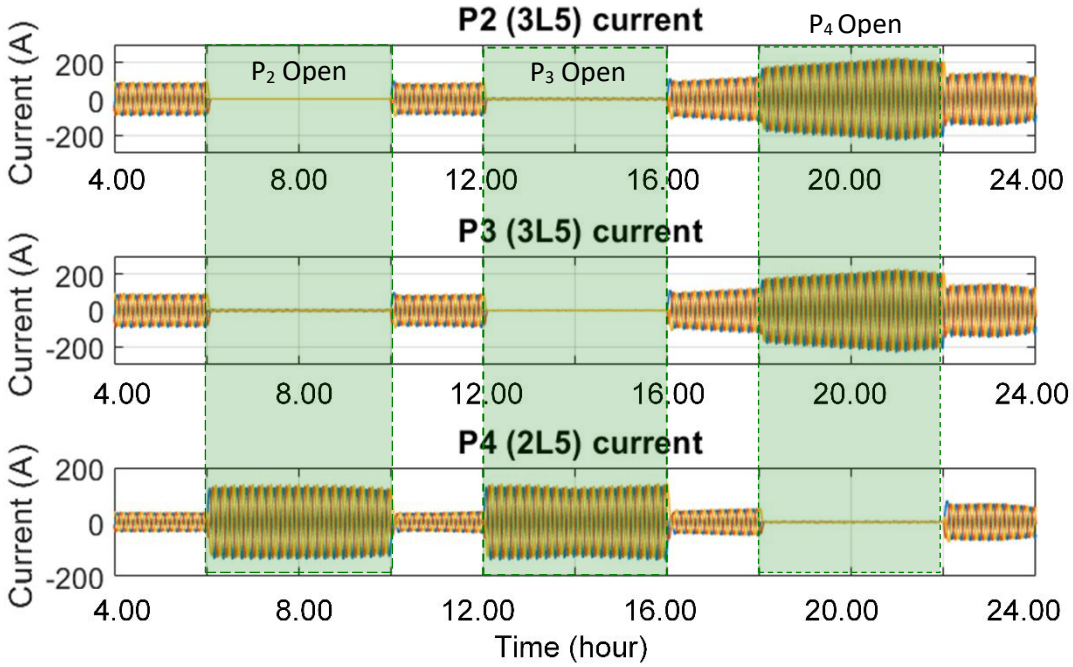

Figure 15: Three-phase current at the circuit breakers under contingency cases.

4.4 THD results with four inverters coordinated

The impact of operation of four inverters on the voltage THD is described in this section. The observation period is the same as in Section 3.4 (October 1st, 2019 – October 3rd, 2019) but all inverters are fed back from P_1. Figure 16 shows the voltage THD at TIVE3 without and with harmonic compensation. The percentage of reduction at the selected points and windows are given in Table 3.

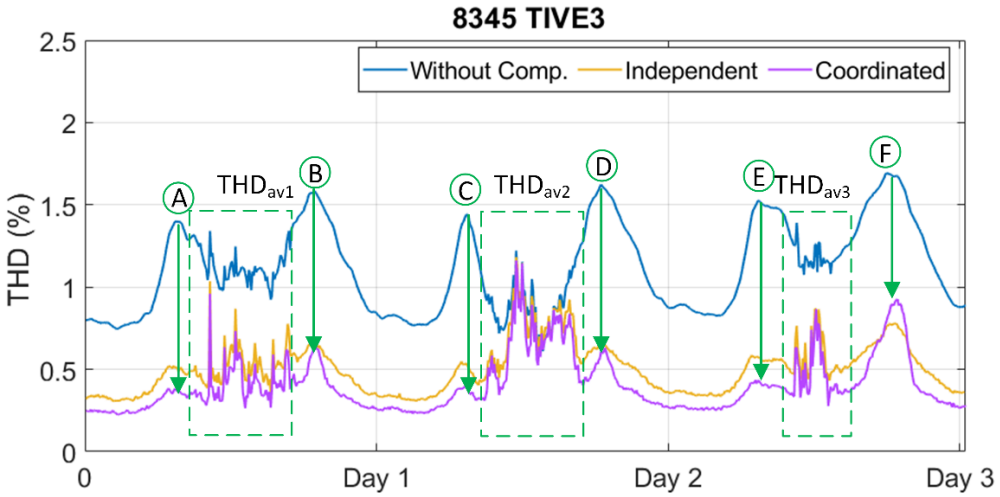

Figure 16: Voltage THD at TIVE3 for three cases: without compensation, with independent operation and with coordinated operation.

Table 3: Voltage THD with and without harmonic compensation deployed at four inverters.

THD voltage profile point	THD Without harmonic compensation	THD with coordinated operation (Figure 16)	Reduction with coordinated operation (%) (Figure 16)	Reduction with independent operation (%) (Figure 4)
A	1.45	0.45	69.0	64.8
B	1.64	0.62	62.1	60.3
C	1.50	0.38	74.6	64.0
D	1.69	0.62	63.3	60.9
E	1.59	0.42	73.6	63.5
F	1.76	0.91	48.4	56.2
THD_{av1}	1.24	0.49	60.6	54.8
THD_{av2}	0.91	0.72	21.1	13.1
THD_{av3}	1.34	0.76	43.3	40.2

4.5 Conclusions

The study of coordinated operation between four inverters resulted in the identification of the most effective current measurement point. It was concluded that when all inverters use P_1 (i.e. the bulk supply point) for current measurement, the highest harmonic compensation can be achieved.

Robustness validation tests proved that the algorithm is functioning as expected under varying operating conditions. During contingency tests, some unexpected results were observed, and these were established to be due to a resonance being excited by small currents from the inverters. This resulted in further fine tuning of the inverter control with the addition of a low-pass filter, details of which are explained in the next section.

5 Updated version of the control algorithm

As a result of the tests applied above, further refinements were applied to the control algorithm, with the effect of improving its performance. The core of the algorithm is the same as developed in WP2, with the following elements added:

- A low-pass filter to remove high-frequency components from the voltage signal measured on the power grid.
- A transformer losses coefficient (k_t) that curtails the harmonic currents to ensure that the transformer losses are kept equal to or below the rated value.

5.1 LPF applied to the input voltage

As a discussed in Section 4.3.1, it was observed that under a contingency condition, harmonic resonances were created in the system, specifically at the 15th order. This phenomenon resulted in amplification of harmonic current components and increased voltage distortion across the system. The control algorithm described in Section 2 did not include any filtering of the input voltage, and therefore this distortion, although in some cases was small, was fed through the controller and was creating additional distortion at the inverter output.

To eliminate the above condition, a LPF was added to the input voltage measurement. The LPF in effect eliminates any distortions on the measured voltage signal above the cut-off frequency (1 kHz), and this in turn stops the inverters in producing any excess harmonics due to internal control loops and switching processes. The MATLAB/Simulink implementation is shown in Figure 17.

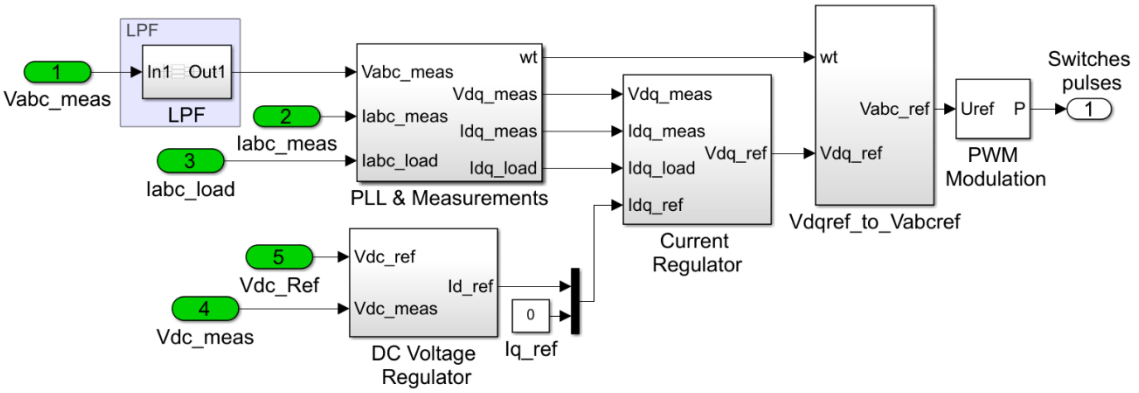

Figure 17: Simulink implementation of the AF control. The LPF added to the voltage measurement is highlighted.

5.2 Transformer losses coefficient

It was observed that when the AF functionality is activated, there is a possibility of the step-up transformer connected to the inverter may experience losses that exceed the rated values [10], [11]. Transformer losses are the combination of fundamental losses (due to fundamental current) and harmonic losses (due to AF functionality). Because of the skin effect, the transformer resistance increases with the frequency, and therefore it is possible that when the inverter is injecting fundamental current and harmonics simultaneously, the transformer losses will exceed the nominal value, even if the rated inverter capacity is not exceeded.

To overcome this issue, a second harmonic injection limiter was developed and added to the main control algorithm (in addition to the automatic gain described in Section 2.2).

In general terms, the transformer losses should always be maintained below the rated value, as expressed in the following equation:

$$I_1^2 R_1 + I_5^2 R_5 + I_7^2 R_7 + I_{11}^2 R_{11} + I_{13}^2 R_{13} \leq I_{1,rated}^2 R_1 \tag{2}$$

where, I_1, I_5, I_7, I_{11}, and I_{13} represent the fundamental and 5th, 7th, 11th and 13th rms current, respectively; R_1, R_5, R_7, R_{11}, and R_{13} are the frequency dependent resistances of the transformer, calculated according to [12].

Dividing all terms of (2) by $I_{1,rated}^2 R_1$ yields:

$$i_1^2 + i_5^2 r_5 + i_7^2 r_7 + i_{11}^2 r_{11} + i_{13}^2 r_{13} \leq 1 \tag{3}$$

where small letters (i_k and r_k) indicate per unit values. Introducing a multiplier k_t (referred to as 'transformer loss coefficient') to further control the level of current harmonic, (3) becomes:

$$i_1^2 + (k_t i_5)^2 r_5 + (k_t i_7)^2 r_7 + (k_t i_{11})^2 r_{11} + (k_t i_{13})^2 r_{13} \leq 1 \tag{4}$$

Then k_t can be solved as:

$$k_t = \sqrt{\frac{1 - i_1^2}{i_5^2 r_5 + i_7^2 r_7 + i_{11}^2 r_{11} + i_{13}^2 r_{13}}} \tag{5}$$

Expression (5) can be rewritten in the dq-reference frame[1] as follows:

$$k_t = \sqrt{\frac{1 - i_d^2}{(i_{d4}^2 + i_{q4}^2)\, r_5 + (i_{d6}^2 + i_{q6}^2)\, r_7 + (i_{d12}^2 + i_{q12}^2)\, r_{13}}} \tag{6}$$

[1] Work package W1b report includes a detailed description of the reference frame calculation.

This coefficient is then multiplied by the harmonics extracted from the load current and adjusts the level of the injected harmonics.

Based on equation (6), k_t is a positive number that theoretically can vary from zero to very large values. Therefore, a limiter (referred to as 'saturation block' in Simulink) is required to avoid numerical instabilities. Various tests were run to assess the impact of the limits on the transformer losses, and it was observed that:

- The lower limit has the largest impact on transformer losses during daytime, when fundamental current output is high. It was found out that a lower limit equal to 0.5 allows controlling the transformer losses to be below the rated value for most operating conditions, with a few exceptions. A lower limit of 0.3 ensures that transformer losses are within the limits for all operating conditions. Therefore, choosing the lower limit is a compromise between the amount of harmonic mitigation carried out, and maintaining the transformer hot-spot temperature within acceptable values.
- The upper limit is reached when fundamental current is small, and therefore there is room in the inverter for injecting high harmonic currents. Various values were tested, and it was observed that when k_t is greater than 1, harmonic compensation increases when compared to coordinated operation. An upper limit equal to 6 was finally chosen, as this value is not reached during the tests, thus maximising compensation.

The MATLAB/Simulink implementation of equation (6) is shown in Figure 18.

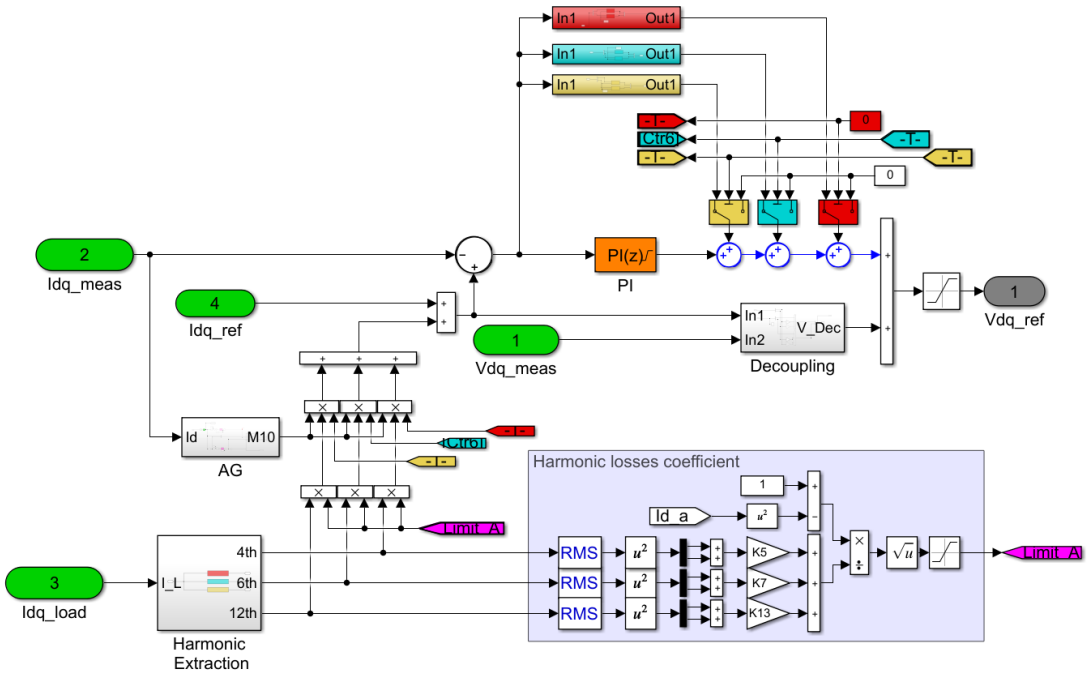

Figure 18: Simulink implementation of current regulation with harmonic losses coefficient (k_t).

5.1.1 Results

In Figure 19 - Figure 21, the transformer losses calculated at three different locations are presented: the first graph shows losses due to the harmonic current, the second graph shows losses due to fundamental current, and the third graph shows the total transformer losses. The rated losses are indicated by a horizontal line. The results indicated that the total losses are within the rated limits for all transformers.

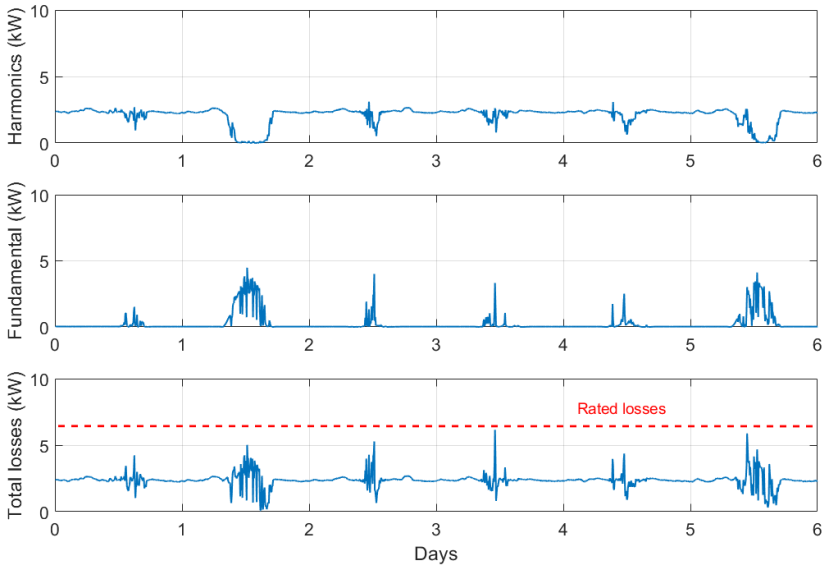

Figure 19: Ayshford transformer losses.

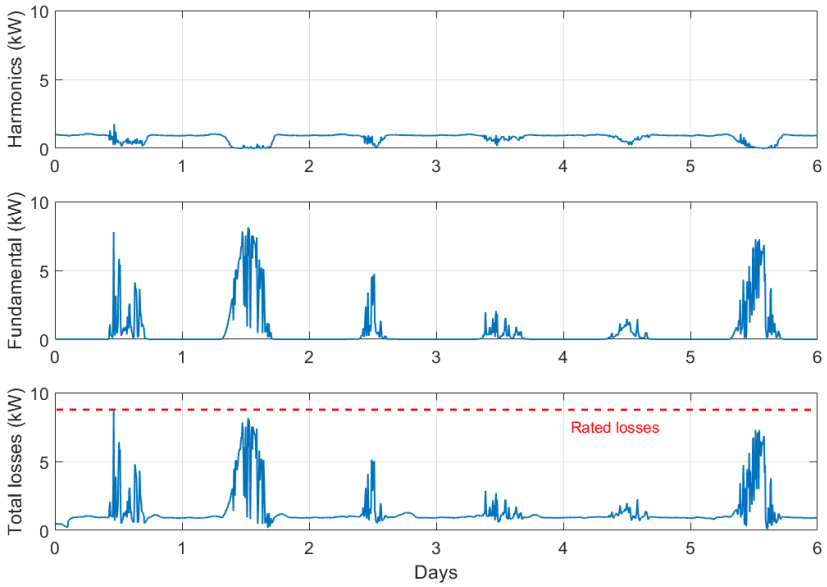

Figure 20: Stoneshill transformer losses.

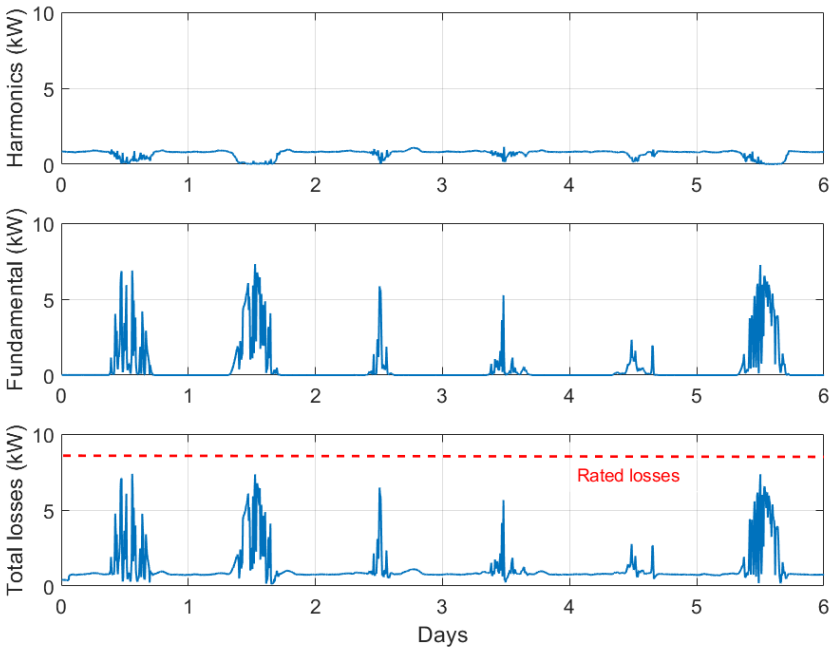

Figure 21: Cullompton transformer losses.

5.3 Updated version of the algorithm

The changes described above resulted in an optimisation and further tuning in the control algorithm. The updated version of the control diagram is shown in Figure 22, and the blocks corresponding to the LPF and the transformer losses coefficient (k_t) are highlighted in yellow.

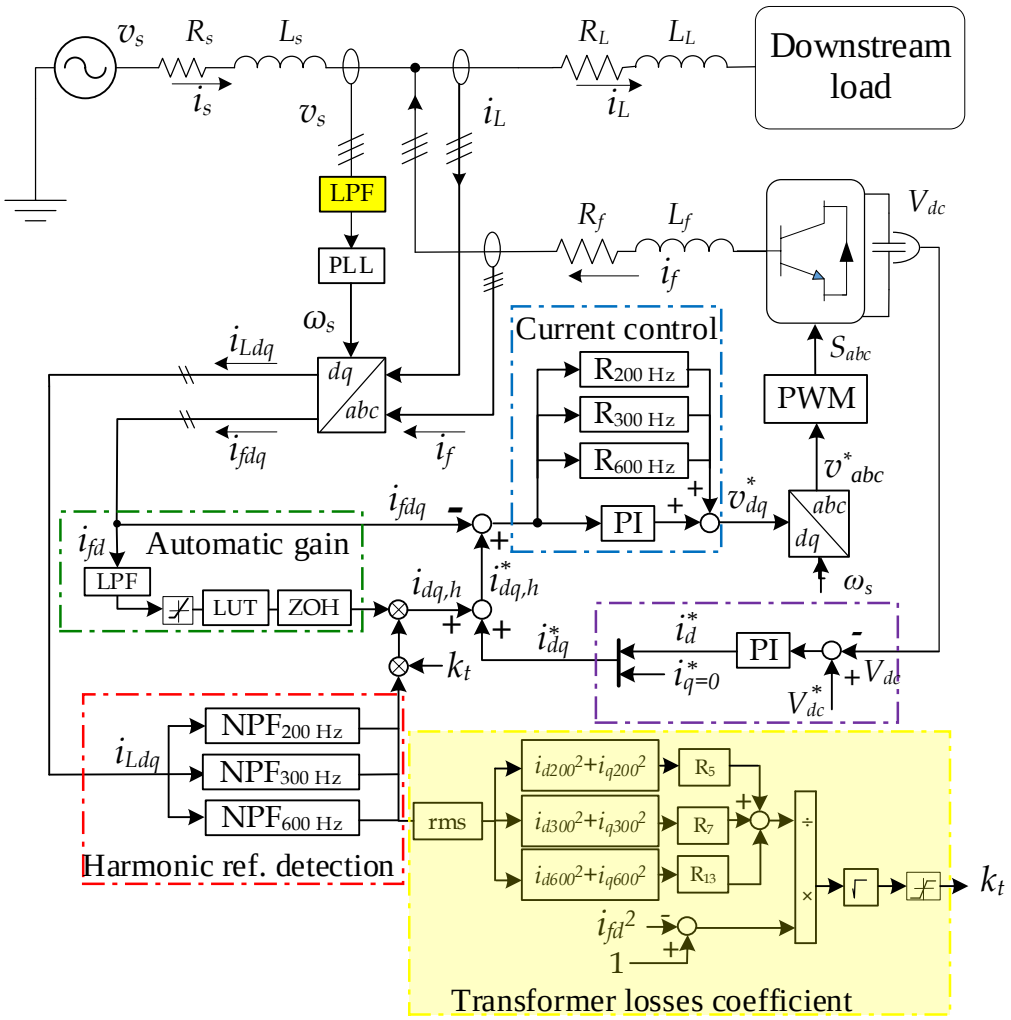

Figure 22: Updated version of the control algorithm: the blocks added as result of optimisation in WP3 are highlighted in yellow.

5.4 THD results with four inverters coordinated and updated control algorithm

Figure 23 shows the voltage THD at TIVE3 without and with harmonic compensation, when k_t lower threshold is equal to 0.3. The percentage of reduction at the selected points and windows are given in Table 4. The behaviour is similar to the one shown in Section 4, however, one can observe that during the day the peak reduction is less compared to Table 3. More detailed comparison between the various cases is carried out in the next section.

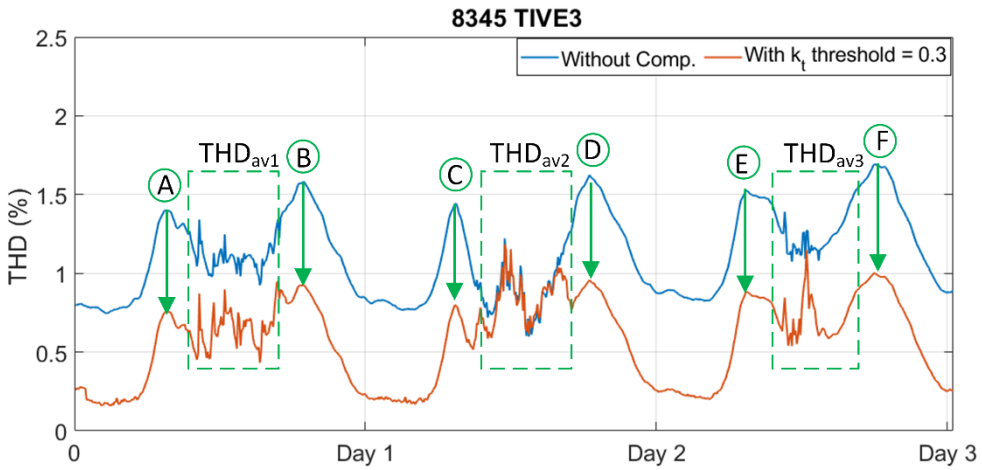

Figure 23: Voltage THD at TIVE3 without compensation and with the latest version of the algorithm.

Table 4: Voltage THD with and without harmonic compensation deployed at four inverters, for the case shown in Figure 23.

THD voltage profile point	Without harmonic compensation	With coordinated operation and k_t=0.3 (Figure 23)	Reduction (%)
A	1.45	0.76	47.5
B	1.64	0.92	43.9
C	1.50	0.79	47.3
D	1.69	0.93	44.9
E	1.59	0.87	45.2
F	1.76	0.99	43.7
THD_{av1}	1.24	0.72	37.0
THD_{av2}	0.91	0.84	7.7
THD_{av3}	1.34	0.80	40.0

5.5 Comparison of THD results for all operating conditions studied in WP3

Figure 24 shows the THD at TIVE3 without compensation and a comparison with the three compensation strategies described in this document: independent (Section 3), coordinated (Section 4), with voltage filter and k_t (Section 5). The comparison in terms of THD reduction is summarised in Table 5.

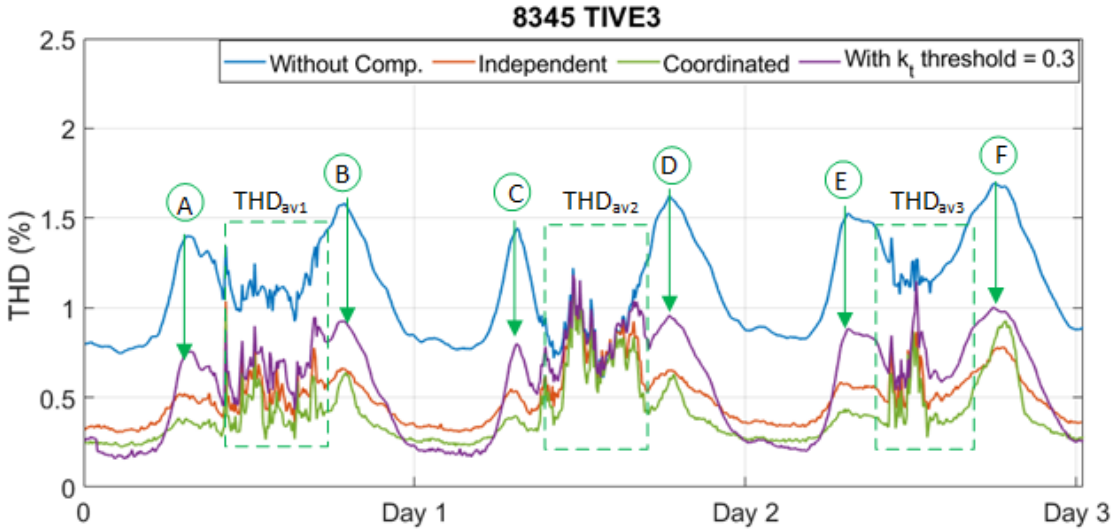

Figure 24: Voltage THD at TIVE3 for the original case, and the three operating conditions studied in WP3.

Table 5: Voltage THD reduction from original value for the three operating conditions studied in WP3.

THD voltage profile point	Voltage THD reduction (%)		
	Independent operation (Section 3, Figure 4)	Coordinated operation (Section 4, Figure 16)	With k_t = 0.3 (Section 5, Figure 23)
A	64.8	69.0	47.5
B	60.3	62.1	43.9
C	64.0	74.6	47.3
D	60.9	63.3	44.9
E	63.5	73.6	45.2
F	56.2	48.4	43.7
THD_{av1}	54.8	60.6	37.0
THD_{av2}	13.1	21.1	7.7
THD_{av3}	40.2	43.3	40.0

The results shown above indicate that coordinated operation leads to the best compensation in terms of reduction of THD peaks and THD average value during the day. At night-time, the THD values with the latest version of the algorithm (k_t lower threshold equal to 0.3) were slightly lower. This was because the coefficient k_t identified additional capacity to inject harmonics compared to the coordinated case, where the transformer loss coefficient was not implemented, as explained in Section 5.2. However, being the THD levels at night time lower than during the day, the impact of introducing k_t was minimal.

It is important to observe that the results presented in Section 4 are achievable in the practice, because in a real implementation, it is expected that multiple inverters within the same PV farm will be able to provide harmonic compensation. Due to computational limits, it was not possible to include multiple inverters at all PV farms in the existing model, and therefore transformer losses due to harmonics were high, in particular at Ayshford.

5.6 Conclusions

The tests carried out in this report resulted in further tuning of the controls, increasing robustness of the control algorithm to resonance conditions, and ensuring that transformer losses are within the rated values.

Transformer loss limitation required further curtailment of harmonic injection, thus resulting in a slightly reduced harmonic compensation when compared to the case studied in Section 4.

6 WP3 Conclusions

A key objective of Work Package 3 was to study the use of multiple inverters on a distribution system to perform harmonic mitigation in a coordinated and optimised way.

To fulfil the key objective, the control algorithm developed in WP2 was deployed at various locations within the given test network. Multiple feedback points were tested to optimise the AF capability of the PV inverters. As expected, the use of multiple inverters to perform harmonic mitigation resulted in further reduction of voltage THD when compared to the case with a single inverter, studied in WP2.

Further tests were introduced to check the robustness and stability of the control algorithm under various scenarios. The results indicated possible issues such as excitation of a resonance by a small inverter harmonic current. This was resolved by introducing a low-pass filter to the input voltage making the overall control algorithm more robust and resilient to possible system-driven events.

An additional control functionality in the form of a limiter was added to control the overall transformer losses (combination of fundamental and harmonic current losses). This was achieved by a coefficient with lower and upper threshold limits multiplied with the harmonic reference currents. Introducing this change resulted in transformer losses not exceeding their rated value under all conditions at the expense of losing some AF compensation capacity from the inverters. In the practice, it is expected that multiple inverters across various PV farms can and will be used for harmonic mitigation, thus allowing higher compensating harmonic injection from individual inverters, and further decrease of the voltage THD.

7 Lessons learned

The following conclusions are drawn:

- The simulation results indicate that the four inverters located at Ayshford (1), Stoneshill (1), and at Cullompton (2) PV farm can be used to perform simultaneous harmonic mitigation.
- For the system under study, the best current measurement point is the bulk supply point, P_1. However, it is possible to have multiple measurement points and modify them, depending on system operating conditions or other events (for example, faults on a feeder). Using a different current measurement point will change the duty on each inverter (both increase and decrease is possible).
- Introduction of a low-pass filter into the input voltage signal results in a more tuned control operation by avoiding voltage harmonics to be fed to the controller and in return causing distortion to the inverter output current.
- The automatic gain and the transformer loss coefficient limit the amount of harmonic current injected. This keeps the overall inverter current and transformer losses within rated levels.
- The inverter has an impact on the equivalent system impedance, in particular at the frequencies of current injection, due to a combination of inverter output filter and control loops. The inverter equivalent impedance changes when AF operation is activated, due to the introduction of additional control loops, compared to normal operation. The impact decreases with increased electrical distance in the point of interest (i.e. where equivalent impedance is calculated).

8 Bibliography

[1] Mathworks Technical Documentation, "Simulink Product Page," [Online]. Available: https://www.mathworks.com/products/simulink.html. [Accessed 12 05 2020].

[2] P. Mattavelli, "Synchronous frame harmonic control for highperformance Performance AC power supliers," *IEEE Transaction of Industrial Applications,* vol. 37, no. 2, p. 864 –872, 2001.

[3] H. A. Pereira, R. M. Domingos, L. S. Xavier, A. F. Cupertino, V. F. Mendes and J. O. S. Paulino, "Adaptive saturation for a multifunctional three-phase photovoltaic inverter," *17th European Conf. on Power Electron. and Appl. (ECCE-Europe),* pp. 1-10, Geneva, 2015.

[4] IEC 61000-4-30:2015 Electromagnetic compatibility (EMC)-Part 4-30, "Testing and measurement techniques - Power quality measurement methods".

[5] X. Yuan, W. Merk, H. Stemmler and J. Allmeling, "Stationary-frame generalized integrators for current control of active power filters with zero steady-state error for current harmonics of concern under unbalanced and distorted operating conditions," *IEEE Trans. Ind. Appl.,* vol. 38, no. 2, p. 523–532, Mar./Apr. 2002.

[6] A. Vidal, F. Freijedo, A. Yepes, P. Fernandez-Gomesana, J. Malvar, O. Lopez and J. Doval-Gandoy, "Assessment and optimization of the transient response of proportional–resonant current controllers for distributed power generation systems," *IEEE Trans. Ind. Electron,* vol. 60, no. 4, p. 1367–1383, Apr. 2013.

[7] R. Teodorescu, F. Blaabjerg, U. Borup and M. Liserre, "A new control structure for grid-connected LCL PV inverters with zero steady-state error and selective harmonic compensation," in *Appl. Power Electron. Conf. and Exp., APEC, Nineteenth Annual IEEE*, vol. 1, 2004, pp. 580–586..

[8] J. Hu, H. Nian, H. Xu and Y. He, "Dynamic modeling and improved control of DFIG under distorted grid voltage conditions," *IEEE Trans. Energy Convers.,* vol. 26, no. 1, p. 163–175, Mar. 2011.

[9] Liao, X. and Wang, X., "Impedance-based stability analysis for interconnected converter system with open-loop RHR poles," *IEEE Transactions on Power Electronics,* vol. 35, no. 4, pp. 4388-4397, 2019.

[10] Western Power Distribution, "Relating to 132kV, 66kV and 33kV medium power transformer rating (Standard SD8C/1)," 2008.

[11] Western Power Distribution, "Dynamic Asset Rating Primary Transformers," 2015.

[12] CIGRE Study Committee B4 and C4, "Technical Brochure 766: Network modelling for harmonic studies," 2019.

Appendix A: Description of the Tiverton network

The main busbar at Tiverton is rated 33 kV and the substation is supplied by two 132/33 kV transformers. The main busbar supplies eight 11 kV busbars (anticlockwise listing):

- Tiverton Moorhays (bus 7735, TIVM5)
- Tiverton South (bus 7737, TIVS5)
- Bridge Mills (bus 7117, BRIM5)
- Cullompton (bus 7236, CULL5)
- Dunkeswell (bus 7271, DUNK5)
- Hemyock (bus 7367, HEMY5)
- Burlescombe (bus 7136, BURL5)
- Tiverton Junction (bus 7733, TIVE5)

The network includes: one radial feeder (Tiverton 33kV, Ayshford Court, Burlescombe, Hemyock, Dunkeswell); two ring circuits (Tiverton 33 kV, Tiverton Moorhays, Tiverton South and Tiverton 33kV), (Tiverton 33 kV, Cullompton Solar Park, Bridge Mills, Cullompton, Stoneshill SP, and Tiverton 33kV); plus Tiverton Junction, directly connected to the Tiverton 33kV bus.

Three solar farms exist within the 33 kV system: Ayshford Court (bus 9370, AYSH3), Stoneshill farm (bus 9850, STFA3) and Cullompton (bus 9830, CMPV3). The main characteristics of the three PV farms are as follows:

Ayshford:

- Connection agreement: Export capacity = 4,550 kVA; import capacity = 50 kVA
- The PV farm includes nine 500 kVA 33/0.4 kV transformers; each transformer connecting to four junction boxes; each junction box connecting up to 7 Siemens Sinvert PVM20 inverters

Cullompton:

- Connection agreement: Export capacity = 4,082 kVA; import capacity = 60 kVA
- The PV farm includes two 2000 kVA 33/0.4 kV transformers; each transformer connecting to one HEC Freesun 1800 kVA inverter

Stoneshill:

- Connection agreement: Export capacity = 4,000 kVA; import capacity = 50 kVA
- The PV farm includes five 33/0.38 kV transformers; each transformer connecting to one 800 kVA inverter.

Appendix B: Impact of different feedback points for individual inverter operation

As described in the document, the current measurement point has an impact on the inverter harmonic currents output. This appendix illustrates the impact of changing the feedback point by illustrating the case of the Stoneshill inverter. The Cullompton inverter is disconnected for this case.

For this test, the 5th harmonic current component only is considered and the results are summarised in Figure 25. In this figure graph, the 5th harmonic rms current magnitude measured at various locations is shown. The busbars where Cullompton PV farm is connected is labelled 'CULL', the busbar where Stoneshill PV farm is connected is labelled 'STON'. The other locations are according to the SLD in Figure 1. The coloured bars indicate various operating conditions:

- Blue: no compensation is applied. The current at P_1 is almost 3.5 A, while there is no harmonic current from Stoneshill.
- Green: the current measurement point is P_1. Stoneshill inverter injects nearly 2.4 A of 5th harmonic, which results in reduction of 5th harmonic at P_1 by 71%
- Yellow: the current measurement point is P_2. Stoneshill inverter injects nearly 1.9 A of 5th harmonic, which results in reduction of 5th harmonics at P_1 by 55%.
- Orange: the current measurement point is P_4. Stoneshill inverter injects 2.3 A of 5th harmonic, which results in 65% reduction of 5th order harmonic measured at P_1.

Changing the current measurement point has the largest impact on the harmonic measurements at P_1 and P_2. However, the harmonic current amplitudes at other locations are affected too, due to varying harmonic current flow in the system.

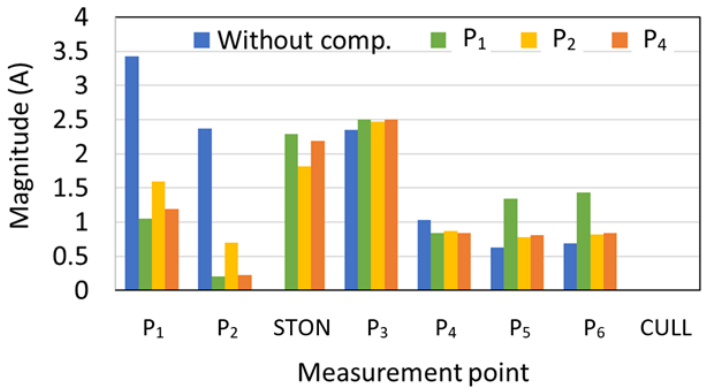

Figure 25: Fifth harmonic current amplitude at different locations without compensation and for varying current measurement points applied at Stoneshill.

From the above discussion, the highest harmonic current reduction is achieved when P_1 is used as a current measurement point. Similar results have been obtained for all inverters and for all harmonic orders considered in this work.

Appendix C: Results with four inverters and k_t lower threshold set to 0.5 and 0.3

This appendix shows the main simulation for the complete observation period (October 1st, 2019 – October 20th, 2019). The results are divided in two sections: system quantities, control quantities and transformer losses.

C.1 Control quantities

The transformer losses coefficient is shown in Figure 26 for Ayshford, Stoneshill and Cullompton, respectively. The transformer losses coefficient upper threshold is fixed to 6, while for the lower threshold two values are tested: 0.5 and 0.3. As one can see, the lower threshold is hit during the day while the upper values of k_t are obtained at night (the label for each day corresponds to 00:00 am). On day 5, the maximum k_t value is reached for all inverters – this corresponds to a condition where small harmonic currents are present in the system, and therefore the inverters can provide large compensation.

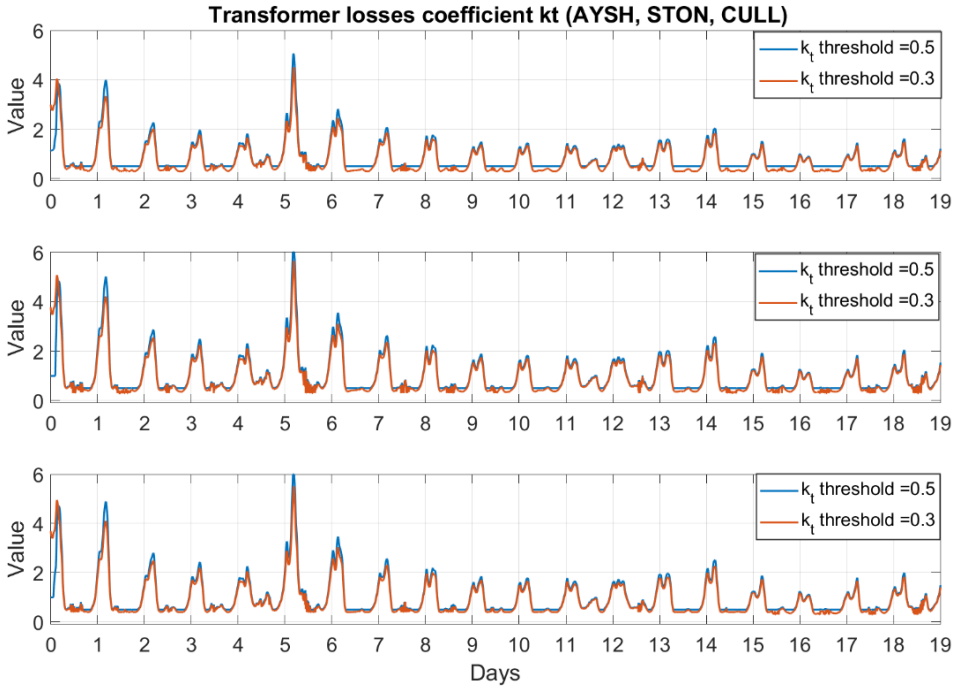

Figure 26: Transformer coefficient (k_t) of the three inverters.

The automatic gain is shown in Figure 27, and varies between 0 and 1. The automatic gain is 1 during night-time, while it decreases during the day. When the inverter output power is equal to the rated value, the automatic gain is equal to 0. It is worth observing that, since the observation period takes place in October, AG is equal to 1 correspond for most of the time, because of low irradiance. Since the three inverters are located in relative close proximity, and experience similar irradiance conditions, the AG profile is very similar.

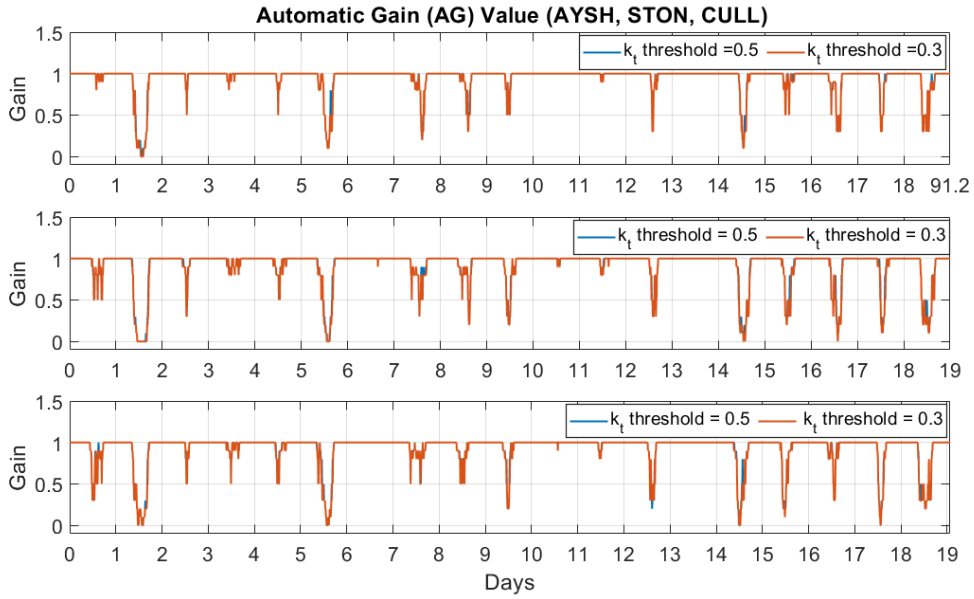

Figure 27 Automatic gain (AG) of the three inverters.

C.2 System quantities

The voltage THD at the BSP is shown in Figure 28 for all cases studied in this report. One can observe that the THD variability is quite regular, and harmonic mitigation is effective throughout the three weeks. The four studied compensation approaches lead to similar improvements in the THD response. This indicates that implementation of the proposed algorithm in individual inverters is expected to provide a visible impact on the system power quality. Further optimisation and tuning leads to incremental improvements.

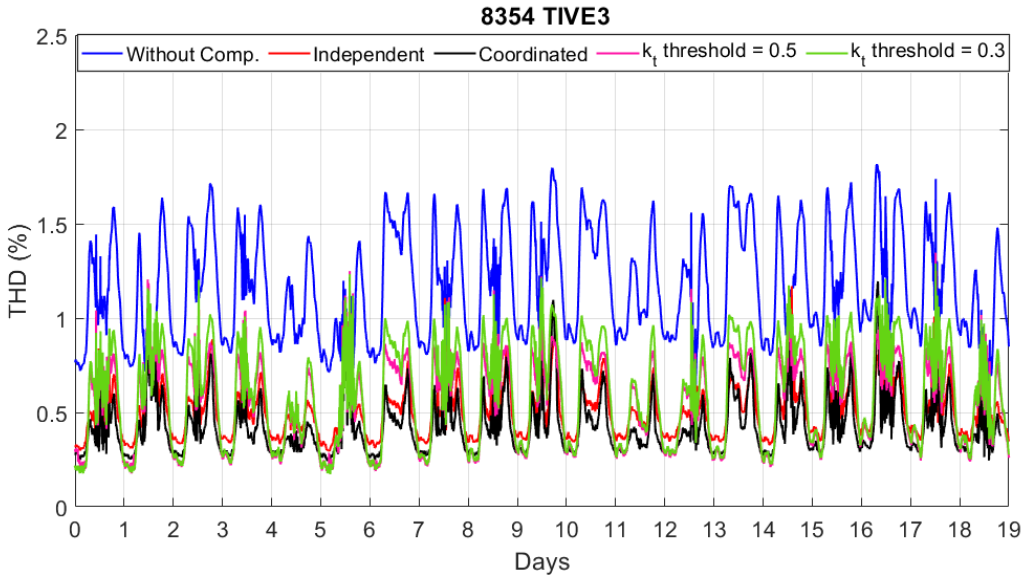

Figure 28: Voltage THD at TIVE3 for various cases.

The inverter rms currents are shown in Figure 29 for two different values of the transformer loss coefficient when the inverter are operating in a coordinated way and P_1 is used as current measurement point. The spikes in inverter current are observed during the day, when fundamental current generation takes place. The impact of changing the value of k_t is more evident at Ayshford. As explained in Section 4, when P_1 is used as current measurement point, Ayshford takes a large harmonic mitigation duty, thus resulting in transformer losses exceeding the rated value under various instances. Reducing k_t threshold results in lower inverter output currents and therefore less transformer losses.

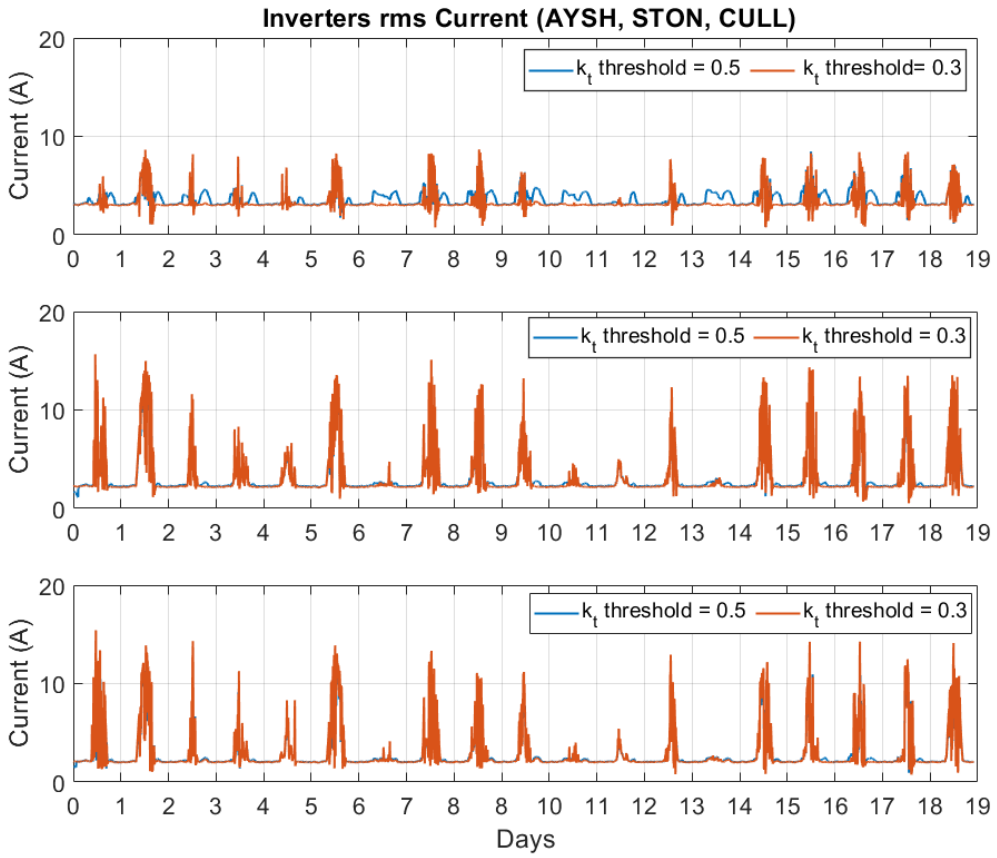

Figure 29: Inverters rms current.

C.3 Transformer losses

The transformer losses reported in Figure 30- Figure 32 are an extended version of the graphs shown in Section 5.1.1. One can observe that the impact of the transformer losses coefficient is more evident at Ayshford, because this inverter is taking on more duties compared to the other inverters connected to the system.

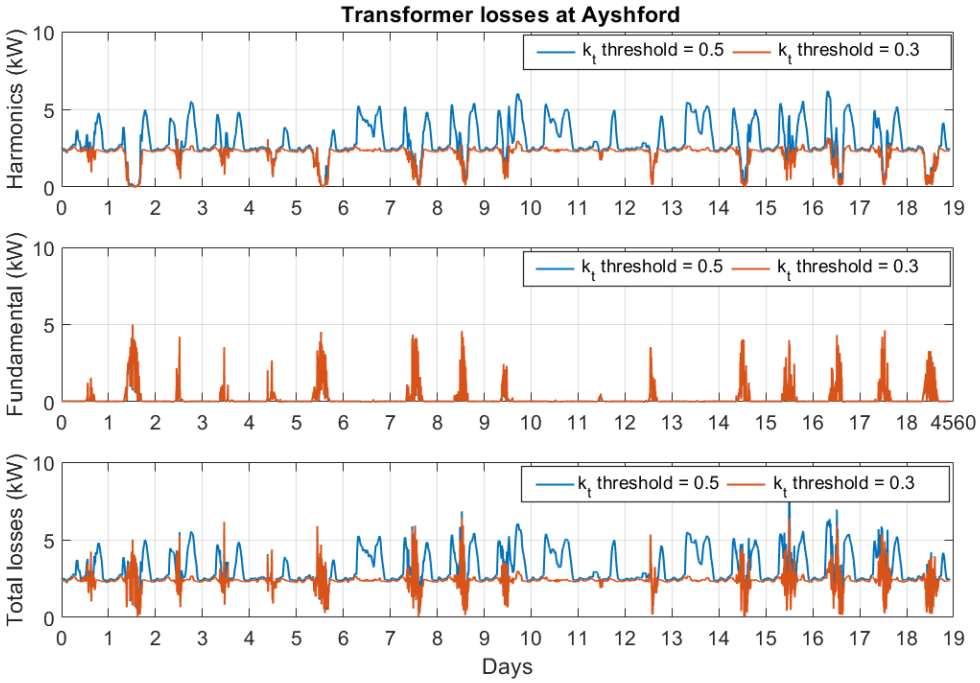

Figure 30: Ayshford transformer losses.

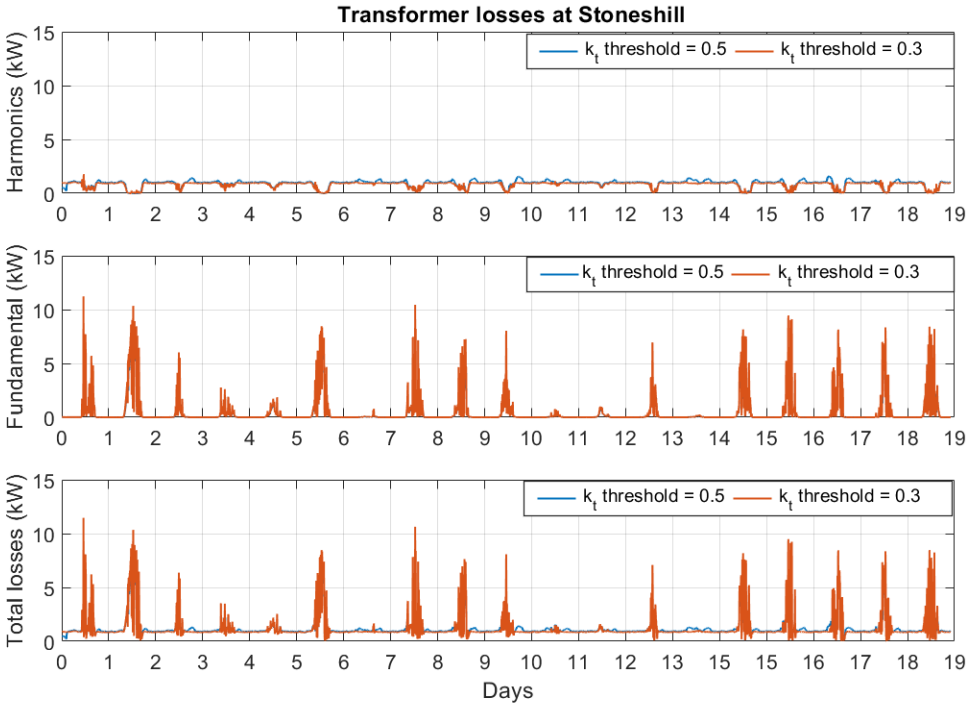

Figure 31: Stoneshill transformer losses.

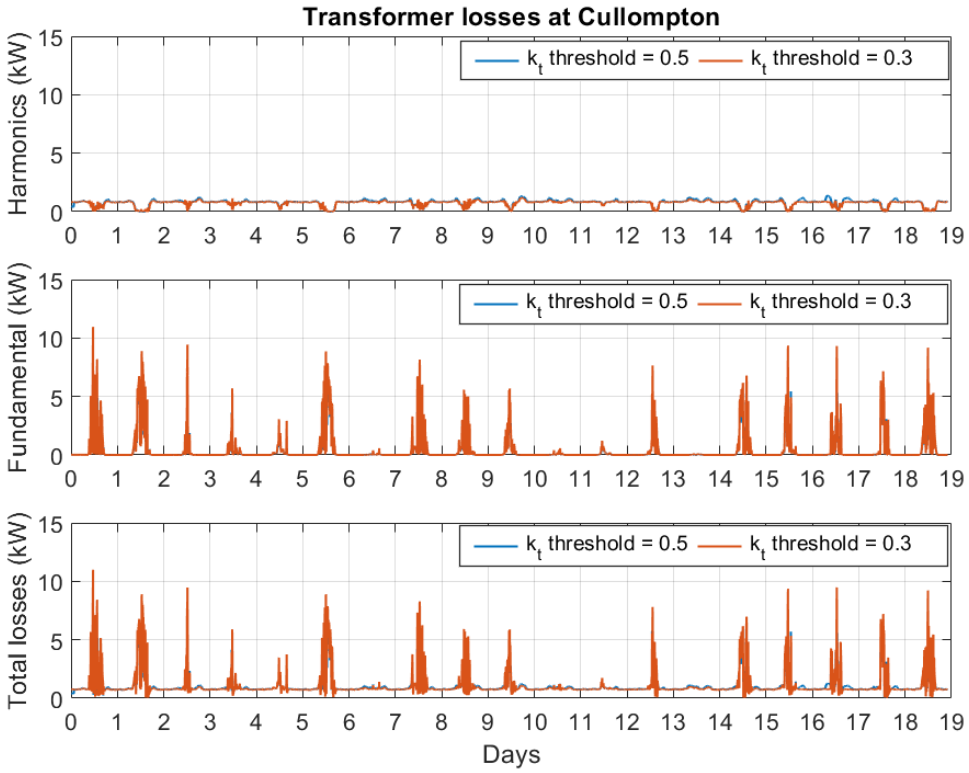

Figure 32: Cullompton transformer losses.